Hindawi
Journal of Chemistry
Volume 2022, Article ID 1346856, 20 pages
https://doi.org/10.1155/2022/1346856

Research Article

ZnO Nanoparticle-Assisted Synthesis of Thiazolo[3,2-α] Pyrimidine Analogs: Antibacterial and Antioxidant Activity, In Silico Molecular Docking, and ADMET Prediction Study

Demis Zelelew,[1] **Milkyas Endale**,[1] **Yadessa Melaku**,[1] **Taye B. Demissie**,[2] **Japheth O. Ombito**,[2] **and Rajalakshmanan Eswaramoorthy**[3]

[1]*Department of Applied Chemistry, School of Applied Natural Science, Adama Science and Technology University, P.O. Box 1888, Adama, Ethiopia*
[2]*Department of Chemistry, University of Botswana, P/Bag UB 00704, Gaborone, Botswana*
[3]*Department of Biomaterials, Saveetha Dental College and Hospital, Saveetha University, Chennai 600 077, India*

Correspondence should be addressed to Demis Zelelew; demis1921zelelew@gmail.com and Milkyas Endale; milkyasendale@yahoo.com

Received 13 August 2022; Revised 10 October 2022; Accepted 13 October 2022; Published 3 November 2022

Academic Editor: Liviu Mitu

In the present study, a new series of nine Thiazolo[3,2-α] pyrimidine analogs were synthesized in good to excellent yields (87.9–96.9%) and improved reaction time using a ZnO nanoparticle-assisted protocol. All the synthesized compounds were characterized using a combination of physicochemical parameters, UV-visible, ^{1}H-NMR, and ^{13}C-NMR spectroscopic methods. Among the synthesized compounds, the in vitro antibacterial activity displayed by compound **16** was higher (14.67 ± 0.58 mm at 500 μg/mL) against *P. aeruginosa* compared to amoxicillin (12.33 ± 0.58 mm at 500 μg/mL), whereas compounds **14** and **18** showed comparable activity (12.00 ± 0.00 mm and 12.33 ± 0.58 mm at 500 μg/mL and 250 μg/mL, respectively) against the same strain. The activities displayed by compounds **14**, **16**, **18,** and **20** were comparable (12.33 ± 1.15 mm, 12.65 ± 0.58 mm, 12.33 ± 0.58 mm, and 12.00 ± 1.00 mm, respectively, at 500 μg/mL) to amoxicillin (13.33 ± 1.15 mm at the same concentration) against *E. coli*. Compound **19** showed good activity (12.00 ± 1.72 mm at 500 μg/mL) against *S. aureus* compared to amoxicillin (16.33 ± 0.58 mm at the same concentration). Compound **19** displayed the highest percent inhibition of DPPH with an IC_{50} value of 9.48 g/mL using the DPPH free radical scavenging assay compared to ascorbic acid (3.21 g/mL) and promising inhibition of peroxide formation (76.28 ± 0.12%), demonstrating its potential in preventing the formation of lipid peroxides. Thus, according to our findings, both the biological activities and in silico computational results revealed that compounds **14**, **16,** and **18** are good antibacterial agents against *P. aeruginosa* and *E. coli*, whereas compound **19** was found to be a promising antibacterial agent against *S. aureus* and an antioxidant agent. The present study revealed that the synthesized compounds appear to be lead compounds for rational drug design.

1. Introduction

Antimicrobial resistance is universally recognized as a serious threat to world health in the 21st century because, in recent decades, there has been a significant increase in the resistance of pathogenic human bacteria to one or more antibiotics [1]. Thus, the search for new drugs is increasing due to the rapid growth of bacterial resistance, which has become a medical concern today because of the rising number of drug-resistant microorganisms [2]. It has been recognized that bactericidal antibiotics induce the formation of toxic reactive oxygen species (ROS) in bacteria, which leads to oxidative damage to DNA, protein, and membrane lipids [3]. The role of ROS in antibiotic-induced bacterial killing is currently a matter of debate and the subject of intense experimental investigation. As a result, the search for novel classes of antibacterial and antioxidants with varied modes of action has become essential in disease prevention

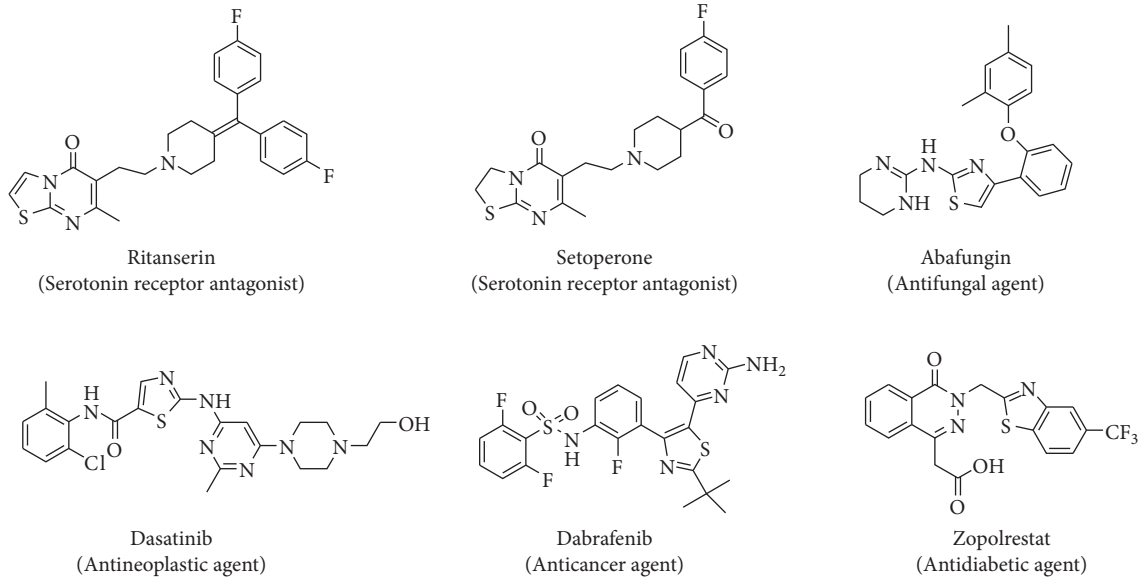

Figure 1: Representative examples of thiazole and pyrimidine-bearing drugs [6–8].

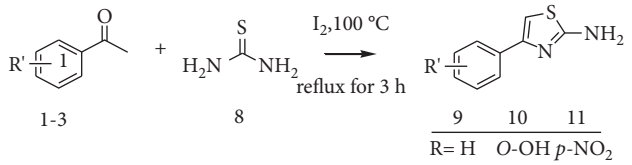

Scheme 1: Synthesis of 2-amino-4-(substituted-phenyl) thiazole derivatives **9**–**11**.

and treatment in light of antibiotic-induced ROS production and its involvement in bacterial resistance.

Natural and semisynthetic flavonoids, particularly chalcones, have received a lot of attention in medicinal chemistry since they possess incredible synthetic utility. Due to the aryl moieties or the enone linker in the chalcones' primary structure, they have undergone several structural alterations [4]. Chalcone-based heterocycles such as Thiazolo[3,2-α] pyrimidine belong to the pseudo-purine class, containing electron-donating (-S-) and electron-accepting (C=N-) groups. Owing to this, they exhibited antibacterial activity and free radical scavenging capacity by delocalization to produce stable DPPH fragments [5]. Hence, systems containing fused thiazole and pyrimidine rings play a significant role in organisms and are underlined by their presence in various drugs available on the market (Figure 1) [6].

These scaffolds are made of bridgehead nitrogen atoms, which are employed continuously and incredibly successfully in a variety of therapeutic applications. Hence, a number of methods were reported for the synthesis of Thiazolo[3,2-α] pyrimidines [7]. However, the majority of the reported strategies have drawbacks, such as extended reaction times, the use of flammable organic solvents, hazardous catalysts, low yields, and harsh reaction conditions. On the other hand, in recent years, nanozinc oxide has gained considerable attention as a heterogeneous catalyst for several organic transformations [8]. The intrinsic Lewis acidity of the zinc ion makes ZnO nanoparticles highly stable and capable of taking on various shapes and sizes. These characteristics were the major factors in their selection for this work.

Herein, we synthesized a new series of Thiazolo[3,2-α] pyrimidine analogs via a ZnO nanoparticles-assisted approach to evaluate their in vitro antibacterial and antioxidant effects, with the ultimate attempt of obtaining new, safer, potent, and comparatively low-cost antibacterial and antioxidant agents. Moreover, in silico molecular docking and ADMET prediction were performed to confirm the binding interaction of the synthesized compounds in the binding pocket of target proteins along with pharmacokinetic and pharmacodynamic profiling, respectively.

2. Materials and Methods

Starting materials, unless otherwise specified in the experimental section, were used as high-analytical grade products. Preliminary chemicals and reagents required to carry out this study were obtained from Merck (Germany), Sigma Aldrich Sigma Chemical, Co. (USA), and Loba Chemie, Pvt. Ltd. (India), which were purchased from commercial suppliers and used directly without further purification unless otherwise noted. Column chromatography was performed using (Merck) Silica gel (particle size 60–120 mm) with *n*-hexanes, ethyl acetate, and dichloromethane as mobile phases. ZnO nanoparticles were obtained from the Department of Applied Chemistry, Material Chemistry research team of ASTU, and they were characterized by UV-Vis, FT-IR spectroscopy, XRD, TEM, PL, and TGA techniques [9]. Amoxicillin and ascorbic acid were used as antibacterial and antioxidant standard drugs, respectively, purchased from EPHARM.

Melting points were determined on a Gallen-Kamp MFB-595 apparatus and are uncorrected. UV spectra were obtained using a double-beam UV-Visible spectrophotometer (Model 2201, India). The ^{1}H NMR and ^{13}C NMR spectra were recorded at 400 and 100 MHz, respectively, on a Bruker Avance III 400 nano by using TMS as an internal standard. The chemical shifts are expressed in δ (ppm) and reported as s (singlet), d (doublet), t (triplet), q (quartet), m (multiplet), dd (doublet of doublets), and brs (broad singlet), respectively. Analytical TLC analysis was performed on precoated aluminum plate silica gel 60 F_{254} (Merck, Darmstadt, Germany). Detection was carried out under UV light (254 and 365 nm). Column chromatographic separations were carried out on silica gel (60–120 mesh, Merck). SwissADME and Autodoc Vina 4.2.6 version software packages were used to undertake in silico ADMET and molecular docking simulation investigations, respectively.

2.1. Synthesis Procedures

*2.1.1. General Synthetic Procedure for the Synthesis of Chalcones (1,3-Diaryl-2-Propen-1-Ones, **5**–**7**).* An equimolar amount of substituted acetophenone derivatives (**1**–**3**) (0.06 mol) and the 2-hydroxy aldehyde (**4**) (0.06 mol) were dissolved in ethanol (5–10 mL), and aqueous NaOH (3 mL, 60%) was added dropwise [10]. The obtained solid products (**5**–**7**) were recrystallized from absolute ethanol to yield a yellow precipitate of chalcone derivatives (S1 Figure 1).

(E)-3-(2-hydroxyphenyl)-1-phenylprop-2-en-1-one (**5**). Orange solid powder; yield: 86.7%; m.p.: 167–169°C; R_f (1% MeOH in petroleum ether = 0.44; ^{1}H-NMR (400 MHz, DMSO-d_6): δ 7.88 (s, OH), 7.50 (d, J = 15.4 Hz, 1H), 7.44 (d, J = 7.5 Hz, 2H), 7.33 (d, J = 15.5 Hz, 1H), 7.03 (t, J = 7.3 Hz, 1H), 6.96 (dd, J = 7.6, 7.2 Hz, 2H), 6.51 (t, J = 7.7 Hz, 1H), 6.18 (d, J = 8.4 Hz, 1H), 5.93 (t, J = 7.4 Hz, 1H); ^{13}C-NMR (101 MHz, DMSO-d_6): δ 190.6, 166.2, 143.9, 139.0, 132.8, 132.6, 130.3, 129.1, 128.5, 122.3, 119.7, 118.1, 115.1.

(E)-1,3-bis(2-hydroxyphenyl)prop-2-en-1-one (**6**). Yellowish solid powder; yield: 92.6%; m.p.: 153–154°C; R_f (1% MeOH in petroleum ether (PE) = 0.44; ^{1}H-NMR (400 MHz, DMSO-d_6): δ 10.80 (s, OH), 8.36 (s, OH), 7.90 (d, J = 8.5 Hz, 1H), 7.85 – 7.77 (m, 1H), 7.74 (d, J = 8.3 Hz, 1H), 7.59 (dd, J = 19.2, 8.5 Hz, 1H), 7.24 (d, J = 7.7 Hz, 1H), 6.98 (t, J = 7.7 Hz, 1H), 6.56 (dd, J = 8.3, 4.9 Hz, 1H);^{13}C-NMR (101 MHz, DMSO-d_6): δ 197.9, 166.9, 158.5, 150.8, 150.3, 148.0, 147.8, 144.3, 141.6, 129.9, 128.0, 127.6, 124.2, 123.9, 123.9.

(E)-3-(2-hydroxyphenyl)-1-(4-nitrophenyl)prop-2-en-1-one (**7**). Reddish solid powder; yield: 94.1%; m.p.: 160–162°C; R_f (1% MeOH in petroleum ether (PE) = 0.44; ^{1}H-NMR (400 MHz, DMSO-d_6): δ 7.98 (s, OH), 7.81 (d, J = 8.4 Hz, 1H), 7.75 (d, J = 8.5 Hz, 1H), 7.66 (d, J = 8.4 Hz, 1H), 7.57 (d, J = 15.7 Hz, 1H), 7.29 (d, J = 15.6 Hz, 1H), 6.82 (t, J = 7.7 Hz, 1H), 6.47 (d, J = 8.2 Hz, 1H), 6.40 (t, J = 7.5 Hz, 1H);^{13}C-NMR (101 MHz, DMSO-d_6): δ 197.8, 167.2, 158.2, 150.2, 149.9, 141.6, 133.1, 129.9, 124.2, 124.1, 121.4, 120.8, 119.8.

*2.1.2. General Synthetic Procedure for the Synthesis of 2-Amino-4-(Substituted-Phenyl)-1,3-Thiazole Derivatives (**9**–**11**).* The thiazole moiety was synthesized by following the Hantzsch's modified method. The rapid and efficient solvent-free reaction of substituted acetophenones (**1**-**3**) derivatives with thiourea (**8**) and iodine under thermal conditions led to 2-Amino-4-arylthiazoles derivatives, **9**–**11** (S1 Figure 2), which were prepared as per literature protocol with slight modifications [11, 12].

4-phenylthiazol-2-amine (**9**). White solid powder; yield: 96.6%; m.p.: 144–146°C; Mol. wt. = 176.24; chemical formula: $C_9H_8N_2S$; R_f (20% EtOAc in n-hexane) = 0.61;^{1}H-NMR (400 MHz, DMSO-d_6): δ 7.35 (d, J = 7.7 Hz, 2H, ArH), 6.94 (t, J = 7.6 Hz, 2H, ArH), 6.84 (d, J = 7.3 Hz, 1H, ArH), 6.55 (s, 1H, CH of thiazole), 2.1 (d, 2H, -NH_2);^{13}C-NMR (100 MHz, DMSO-d_6): δ 168.7, 150.2, 135.1, 128.9, 127.7, 125.9, 102.0.

4- (4-Nitrophenyl) thiazol-2-amine (**10**). Orange solid powder; yield: 86.6%; m.p.: 269.2–270.8°C; Mol. wt = 221.03; chemical formula: $C_9H_7N_3O_2S$; R_f (20% EtOAc in n-hexane) = 0.44;^{1}H-NMR (400 MHz, DMSO-d_6): δ 7.82 (d, J = 8.7 Hz, 2H, ArH), 7.62 (d, J = 8.7 Hz, 2H, ArH), 6.96 (s, 1H, CH of thiazole), 6.77 (d, J = 8.2 Hz, 2H), 2.11 (d, J = 2.0 Hz, 2H,-NH_2);^{13}C-NMR (100 MHz, DMSO-d_6): δ169.1, 148.2, 146.3, 141.1, 126.7, 124.4, 107.1.

2-(2-aminothiazol-4-yl) phenol (**11**). Pale yellow solid powder; yield: 43.2%; m.p.: 138–142°C; Mol. wt = 192.04; chemical formula: $C_9H_8N_2OS$; R_f (20% EtOAc in n-hexane) = 0.73; ^{1}H-NMR (400 MHz, DMSO-d_6): δ 11.56 (s, 1H, OH), 7.24 (d, J = 7.7 Hz, 1H, ArH), 7.00 (s, 1H, CH of thiazole), 6.70 (t, J = 7.7 Hz, 1H, ArH), 6.61 (d, 1H, ArH), 6.38 (t, J = 8.1 Hz, 1H, ArH), 2.09 (d, J = 2.7 Hz, 2H,-NH_2); ^{13}C–NMR (100 MHz, DMSO-d_6):δ 168.6, 155.5, 147.3, 129.3, 126.4, 119.3, 118.4, 117.1, 100.8.

*2.1.3. General synthetic procedure for the synthesis of 5H-Thiazolo [3,2-α] pyrimidine analogs in the presence of ZnO nanoparticles as a catalyst derived from chalcone (**12**–**20**).* A solution of substituted 2-amino-4-substituted phenylthiazole, **9**–**11** (1.5 mmol) in ethanol (20 mL) was mixed with the appropriate α, β-unsaturated ketones, **5**–**7** (1.5 mmol) in the presence of Na metal (0.5 g) under the use of ZnO nanoparticles as a catalyst (0.43 mg, 0.2 mmol, 20 mol %) as depicted in Scheme. The mixture was heated under reflux for 8 hours, and then the solvent was evaporated under a vacuum. The residue was dissolved in chloroform and washed with water. The organic layer was separated, dried, and evaporated. The obtained solid was recrystallized from ethanol to yield Thiazolo[3,2-α] pyrimidine analogs, **12**–**20** (S1 Figure 3). The ^{1}H-NMR spectra of target compounds **12**–**20** revealed the presence of singlet peak (1H) at δ 12.0–10.0 and 7.8 of hydroxyl and thiazole protons, and the spectrum shows a singlet signal at δ 5.4–6.9 assigned to the C-H Thiazolo pyrimidine proton (pyrimidine H-4) and δ 7.4 for methine proton, and the aromatic region shows multiplet at δ 6.9–7.5, indicating the aromatic C-H linkage. The ^{13}C–NMR shows a characteristic peak at δ 167.0–168.0 corresponding to C-2 of thiazole ring. The peak appeared around δ 195.7-168.0 corresponding to (-S-C(N)=N- of

Thiazolo pyrimidine. The appearance of this downfield shift around δ 43.9 for the pyrimidine H-4 indicates the effect of the environment around carbon-4 (aromatic environment) and, consequently, has assigned target structures for the reaction products. As a result, distinct chemical shift positions resonated with these protons. This change in the structure of the scaffold is caused by a change in the substituent position of thiazole and chalcone phenyl groups, which causes different chemical shift values. The ^{1}H and ^{13}C–NMR spectral data of all the synthesized compounds are presented in S2 Figure 5 (1–30), respectively.

2-(3, 7-diphenyl-*5H*-Thiazolo[3,2-α] pyrimidin-5-yl) phenol (**12**). Brown cream solid powder; yield: 87.9%; m.p.: 166–167 °C; Mol. wt = 382.48; chemical formula: $C_{24}H_{18}N_2OS$; R_f (1% MeOH in petroleum ether (PE) = 0.44; UV-Visible (MeOH) λmax = 290 and 420 nm;^{1}H–NMR (400 MHz, DMSO-d_6):δ 9.09 (s, OH), 7.68 (s, 1H, Ar-H of thiazole-H), 7.47 (s, 1H, CH=C), 7.15–6.93 (m, 1H), 6.92 (d, J = 7.7 Hz, 1H), 6.81 (d, J = 7.9 Hz, 1H), 6.65 (d, J = 7.8 Hz, 1H), 6.63- 6.52 (m, 1H), 6.52–6.45 (m, 1H), 6.38 (dd, J = 17.2, 8.4 Hz, 2H), 6.31 (dd, J = 13.9, 7.7 Hz, 3H), 6.24 (dd, J = 13.0, 6.9 Hz, 2H), 6.01 (d, J = 7.8 Hz, 1H), 5.99–5.60 (m, 1H), 4.66 (s, 1H, benzylic-H);^{13}C–NMR (100 MHz, DMSO-d_6):δ 200.6, 168.9, 164.8, 161.0, 150.3, 144.4, 135.1, 133.0, 132.3, 129.5, 129.1, 129.0, 128.5, 127.8, 126.7, 125.9, 125.7, 119.2, 116.9, 102.2, 49.1.

2-(5-(2-hydroxyphenyl)-7-phenyl-*5H*-Thiazolo[3,2-α] pyrimidin-3-yl)phenol (**13**). Brown solid powder; yield: 92.1%; m.p.: 168–169°C; Mol. wt = 398.48; chemical formula: $C_{24}H_{18}N_2O_2S$; R_f (1% MeOH in petroleum ether (PE) = 0.44; UV–Visible (MeOH) λ_{max} = 290 and 320 nm; ^{1}H–NMR (400 MHz, DMSO-d_6): δ 10.40 (s, OH), 8.96 (s, 1H, Ar-H of thiazole-H), 7.42 (s, 1H, CH=C), 7.20 (d, J = 10.1 Hz, 1H), 6.89 (d, J = 7.4 Hz, 1H), 6.74 (d, J = 7.7 Hz, 1H), 6.33 (m, J = 8.8, 5.0 Hz, 2H), 6.24 (d, J = 7.7 Hz, 2H), 5.73 (d, J = 7.6 Hz, 2H), 4.71 (s, 1H, benzylic-H);^{13}C–NMR (100 MHz, DMSO-d_6):δ 192.5, 177.5, 173.3, 171.7, 168.5, 162.3, 161.3, 139.4, 136.7, 132.8, 130.85, 130.1, 129.6, 129.2, 128.5, 128.1, 124.8, 120.1, 117.7, 116.5, 49.2.

2-(3-(4-nitrophenyl)-7-phenyl-*5H*-Thiazolo[3,2-α] pyrimidin-5-yl)phenol (**14**). Brown cream solid powder; yield: 96.3%; m.p.: 173–174°C; Mol. wt = 427.48; chemical formula: $C_{24}H_{17}N_3O_3S$; R_f (1% MeOH in petroleum ether (PE) = 0.44; UV–Visible (MeOH) λmax = 290 and 390 nm;^{1}H–NMR (400 MHz, DMSO-d_6): δ 14.78 (s, OH), 7.83 (s, 1H, Ar-H of thiazole-H), 7.66 (d, J = 8.5 Hz, 1H), 7.45 (d, J = 8.6 Hz, 1H), 7.29 (d, J = 7.3 Hz, 2H), 7.11 (dd, J = 14.7, 8.0 Hz, 1H), 7.02 (d, J = 8.2 Hz, 1H), 6.84–6.56 (m, 4H), 6.47 (d, J = 7.6, 6.9 Hz, 1H), 6.24- 6.11 (m, 1H), 6.13–5.97 (m, 1H), 5.91 (s, 1H), 5.06 (s, 1H, CH=C), 4.57 (s, 1H, benzylic-H);^{13}C–NMR (100 MHz, DMSO-d_6):δ 176.8, 171.2, 169.1, 167.9, 162.1, 160.7, 150.1, 148.0, 146.3, 141.0, 139.4, 130.9, 129.6, 129.4, 127.7, 126.6, 124.4, 116.2, 112.8, 107.1, 48.9.

2-(7-(4-nitrophenyl)-3-phenyl-*5H*-Thiazolo[3,2-α] pyrimidin-5-yl)phenol (**15**). Grayish solid powder; yield: 94.1%; m.p.: 171-172°C; Mol. wt = 427.48; chemical formula: $C_{24}H_{17}N_3O_3S$; R_f (1% MeOH in petroleum ether (PE) = 0.44; UV–Visible (MeOH) λmax = 290 and 350 nm; ^{1}H–NMR (400 MHz, DMSO-d_6):δ 9.90 (S, OH), 7.45 (s, 1H, Ar-H of thiazole-H), 7.30 (d,, J = 8.2 Hz, 1H), 6.86 (dd, J = 43.0, 7.6 Hz, 2H), 6.66 (dd, J = 25.9, 8.3 Hz, 2H), 6.61-6.47 (m, 1H), 6.39 (dt, J = 13.4, 6.5 Hz, 4H), 6.37–6.16 (m, 3H), 6.02 (d, J = 7.4 Hz, 3H), 5.62 (d, J = 8.5 Hz, 3H), 5.50 (d, J = 8.1 Hz, 1H), 5.08 (s, 1H, CH=C), 4.67 (s, 1H, benzylic-H); ^{13}C–NMR (100 MHz, DMSO-d_6):δ 196.3, 171.2, 168.8, 167.9, 154.1, 150.1, 135.1, 131.1, 131.0, 129.7, 129.5, 128.9, 127.8, 127.7, 126.7, 125.9, 125.1, 113.0, 102.1, 49.0.

2-(5-(2-hydroxyphenyl)-7-(4-nitrophenyl)-*5H*-Thiazolo [3,2-α] pyrimidin-3-yl)phenol (**16**). Grayish solid powder; yield: 91.6%; m.p.: 183-184°C; Mol. wt = 443.47; chemical formula: $C_{24}H_{17}N_3O_4S$; R_f (1% MeOH in petroleum ether (PE) = 0.44; UV–Visible (MeOH) λmax = 290 and 385 nm; ^{1}H–NMR (400 MHz, DMSO-d_6): δ 15.21 (s, 1H), 7.99 (s, 1H Ar-H of thiazole-H), 7.80 (s, 1H, CH=C), 7.39 (dt, J = 18.2, 9.1 Hz, 1H), 7.24 (t, J = 8.9 Hz, 3H), 7.16 (d, 1H), 7.14 (s, 1H), 6.93–6.71 (m, 1H), 6.62–6.46 (m, 1H), 6.22 (t, J = 7.8 Hz, 2H), 6.14 (d, J = 8.4 Hz, 2H), 6.02 (d, J = 8.2 Hz, 1H), 5.35 (d, J = 181.7 Hz, 3H), 4.70 (s, 1H, benzylic-H);^{13}C–NMR (100 MHz, DMSO-d_6): δ 196.2, 172.5, 167.5, 162.5, 154.0, 150.1, 132.2, 131.1, 131.0, 130.5, 125.2, 117.0, 116.2, 113.0, 112.8, 49.0.

2-(3,7-bis(4-nitrophenyl)-*5H*-Thiazolo[3,2-α] pyrimidin-5-yl)phenol (**17**). Brown solid powder; yield: 90.8%; m.p.: 198–199°C; Mol. wt = 472.47; chemical formula: $C_{24}H_{16}N_4O_5S$; R_f (1% MeOH in petroleum ether (PE) = 0.44; UV–Visible (MeOH) λmax = 290 and 365 nm;^{1}H–NMR (400 MHz, DMSO-d_6): δ 9.37 (s, OH), 7.81 (s, 1H, Ar-H of thiazole-H), 7.61 (s, 1H, CH=C), 7.07 (d, J = 8.4 Hz, 2H), 7.00 (d, J = 8.1 Hz, 2H), 6.97 (d, J = 8.3 Hz, 2H), 6.92 (d, 1H), 6.42 (t, J = 7.2 Hz, 4H), 6.00 (d, J = 8.1 Hz, 2H), 5.88 (d, J = 8.2 Hz, 1H), 5.43-5.02 (m, 1H), 4.55 (s, 1H, benzylic-H);^{13}C–NMR (100 MHz, DMSO-d_6):δ196.7, 177.2, 172.5, 171.2, 168.2, 161.0, 154.2, 150.3, 147.3, 132.2, 131.3, 131.2, 127.7, 127.2, 125.3, 122.2, 114.1, 113.2, 113.0, 49.2.

2-(5-(2-hydroxyphenyl)-3-phenyl-*5H*-Thiazolo[3,2-α] pyrimidin-7-yl)phenol (**18**). Reddish brown solid powder; yield: 96.9%; m.p.: 178–179°C; Mol. Wt=398.48; chemical formula: $C_{24}H_{18}N_2O_2S$; R_f (1% MeOH in petroleum ether (PE) = 0.44; UV–Visible (MeOH) λ_{max} = 290 and 420 nm; ^{1}H–NMR (400 MHz, DMSO-d_6): δ 8.30 (s, OH), 8.19 (s, OH), 7.97 (s, 1H, Ar-H of thiazole-H), 7.78 (s, 1H, CH=C), 7.41 (d, J = 7.2 Hz, 2H), 7.37–7.25 (m, 1H), 7.21 (d, J = 8.5 Hz, 1H), 7.15 (dd, J = 12.0, 8.3 Hz, 1H), 7.01–6.82 (m, 4H), 6.79 (d, J = 7.6 Hz, 1H), 6.72 (d, J = 7.4 Hz, 1H), 6.53 (s, 1H, CH=C), 6.58–6.46 (m, 2H), 6.00 (d, J = 8.1 Hz, 1H), 5.12 (s, 1H, benzylic-H);^{13}C–NMR (100 MHz, DMSO-d_6): δ 167.6, 131.1, 129.4, 128.9, 127.8, 127.7, 126.7, 125.9, 125.2, 113.0, 112.8, 79.40, 49.0.

2-(5-(2-hydroxyphenyl)-3-phenyl-*5H*-Thiazolo[3,2-α] pyrimidin-7-yl)bisphenol (**19**). Brown solid powder; yield: 94.5%; m.p.: 189–190°C; Mol. wt = 414.48; chemical formula: $C_{24}H_{18}N_2O_3$; R_f (1% MeOH in petroleum ether (PE) = 0.44; UV–Visible (MeOH) λmax = 290 and 420 nm;^{1}H–NMR (400 MHz, DMSO-d_6): δ 8.31 (s, OH), 7.99 (s, 1H, Ar-H of thiazole-H), 7.45 (dt, J = 25.8, 7.1 Hz, 1H), 7.37 (s, 1H, CH=C), 7.31–7.09 (m, 5H), 6.56–6.44 (m, 1H), 6.25–5.99 (m, 5H), 5.56 (d, 2H), 5.11 (s, 1H, benzylic-H);^{13}C–NMR (100 MHz, DMSO-d_6):δ 196.2, 167.4, 154.0, 146.6, 139.1,

132.2, 131.1, 130.5, 129.1, 128.1, 125.2, 117.0, 116.2, 113.7, 113.0, 49.0, 38.9.

2-(5-(2-hydroxyphenyl)-3-(4-nitrophenyl)-*5H*-Thiazolo [3,2-α] pyrimidin-7-yl) phenol (**20**). Reddish brown solid powder; yield: 90.8%; m.p.: 192-193°C; Mol. wt = 443.47; chemical formula: $C_{24}H_{17}N_3O_4S$; R_f (1% MeOH in petroleum ether (PE) = 0.44; UV–Visible (MeOH) λmax = 290 and 420 nm; ^{1}H–NMR (400 MHz, DMSO-d_6): δ 8.32 (s, OH), 7.99 (s, 1H, Ar-H of thiazole-H), 7.60 (q, J = 8.0 Hz, 1H), 7.41 (dd, J = 19.1, 8.0 Hz, 1H), 7.33–7.17 (m, 3H), 7.19–7.06 (m, 1H), 6.55 (t, J = 9.1 Hz, 1H), 6.14 (d, J = 8.5 Hz, 3H), 6.02 (d, J = 8.1 Hz, 1H), 5.57 (s, 1H, CH=C), 5.11 (s, 1H, benzylic-H); ^{13}C–NMR (100 MHz, DMSO-d_6): δ 196.2, 167.4, 154.0, 131.1, 125.2, 118.4, 113.6, 113.0, 79.4, 49.0.

2.2. Biological Activity Evaluations

2.2.1. In Vitro Antibiotic Susceptibility Test. The antibacterial susceptibility of each bacterial strain to all the synthesized compounds was assessed using the agar disc diffusion method, as per the CLSI standard protocols [13]. These compounds were individually tested against two Gram-positive bacteria, *S. aureus* (ATCC 29213) and *S. pyogenes* (ATCC 27853), and Gram-negative bacteria, *E. coli* (ATCC 25922) and *P. aeruginosa* (ATCC 27853). The bacterial strains were obtained from the Adama Public Health Research & Referral Laboratory Center. The bacterial strains' identities were recognized and validated using colony morphology and Gram staining, as well as routine biochemical tests, as described in Bergey's Manual of Determinative Bacteriology [14]. The bacterial strains were brought to the microbiology lab with nutrient agar and kept at 4°C until they were needed. Microbial cultures were cultured in nutrient broth overnight at 37°C, adjusted to 0.5 McFarland standards with distilled water, and then inoculated onto Mueller-Hinton agar plates. The tested compounds were freshly dissolved in 1 mL of DMSO and adjusted to a concentration of 250 and 500 μg/mL. After incubation, the test organism was inoculated into the Muller-Hinton agar medium using a sterile cotton swab. Then sterile filter paper (6 mm diameter) was soaked in 1 mL DMSO solution of the compounds at 250 and 500 μg/mL concentrations, separately loaded with 10 μl of prepared compounds, along with the positive and negative controls, and left till dryness, and then positioned on a previously inoculated nutrient agar with the target microbial strain. After two hours of diffusion at 4°C, the plates were incubated at 37°C for 24 h. Antibacterial activity was evaluated by measuring the zone of inhibition against the test organisms and comparing it to amoxicillin as a reference drug at 25 and 50 mg/ml, respectively, while the negative control was DMSO. The experiments were performed in three separate trials, and the average inhibition zone around each compound was measured with a caliper in (mm) [15].

2.2.2. In Vitro Antioxidant Activities Using DPPH Assay. The ability of the synthesized compounds to donate protons or electrons was determined by bleaching the purple color of a methanolic solution of DPPH. The in vitro radical consumption activity of the synthesized compounds was assessed using the reported method [16]. The blank reading solution was methanol, while the standard solution was ascorbic acid, which was calculated by the following equation:

$$\%\ \text{DPPH free radical Scavenging activity} = \frac{A_{blank} - A_{sample}}{A_{blank}} \times 100, \quad (1)$$

where A_{blank} is the absorbance of the control reaction, and A_{sample} is the absorbance of the test sample. Various concentrations of the tested compounds in methanol ranging from 12.5 to 200 g/mL were added to a methanolic solution of DPPH to determine the IC_{50} values. All experiments were carried out in three separate trials to calculate the mean and standard deviation statistically.

2.2.3. In Vitro Lipid Peroxidation Inhibition Assay. The lipid peroxidation inhibition assay was conducted according to the procedure described with a few modifications [17]. Ascorbic acid was used as a reference. The percentage of inhibition was calculated from the following equation:

$$\%\ \text{Lipid peroxidation inhibition} = \frac{A_{control} - A_{compound}}{A_{compound}} \times 100, \quad (2)$$

where A_{compound} = absorbance of the compound, and A_{control} = absorbance of control. To determine the concentration necessary to achieve 50% inhibition of phospholipid oxidation (IC_{50}) in linoleic acid. The percentage of lipid peroxidation inhibition was plotted against the concentration of the synthesized compounds.

2.2.4. In Silico Computational Studies

(1). Pharmacokinetics (ADMET) and Drug-Likeness Prediction Properties. The in silico ADMET prediction helps to understand whether a particular drug has properties suitable for being an orally active drug. This prediction is based on the already established concept of the Lipinski rule of five [18] and the Veber rule [19]. The physicochemical and pharmacokinetics properties of the compounds were estimated using ADME descriptors by SwissADME (http://www.swissadme.ch/), Molinspiration (https://www.molinspiration.com/), and PreADMET (https://preadmet.webservice.bmdrc.org/) online servers. To estimate in silico and pharmacokinetic parameters and other molecular properties, the synthesized compound structures were submitted to SwissADME tools and converted to their canonical simplified molecular-input line-entry system "SMILEs" [20]. The organ toxicity profiles and toxicological endpoints of the ligands and toxicity classes were predicted using the Pro Tox II web server explore (https://tox-new.charite.de/).

(2) Molecular Docking Study. A molecular docking study was performed to investigate the binding mode between the most potent compounds against target proteins. The chemical structures of the compounds plotted with the ChemOffice

tool (Chem Draw 16.0) were indicated with appropriate 2D orientation and the energies of each molecule were minimized using ChemBio3D. Docking simulations were then performed using the energy-minimized ligand molecules as input to AutoDock Vina. Protein and ligand preparations were performed according to standard reported protocols using the Autodock 4.2.6 tool [21]. The DNA gyrase B (PDB ID: 6f86), the *N*-terminal domain of PqsA in complex with 6-fluoroanthraniloyl-AMP (PDB ID:5oe3), Pyruvate Kinase in complex with bis-indole alkaloid (PDB ID:3t07), LuxS of *S. pyogenes* (PDB ID: P0C0C7) and human peroxiredoxin 5 (PDB ID: 1hd2) crystal structures were obtained from the Protein Data Bank to investigate the interaction of the synthesized compounds with the active site of protein targets using the following grid box parameters (PDB ID: 6f86) [62 × 30 × 64], [15 × 14 × 19], (PDB ID:5oe3) [38x-2x17], [19 × 21 × 14], (PDB ID:3t07) [-15x-3x2], [18 × 14 × 16], (PDB ID: P0C0C7) [46 × 45 × 39], [14 × 12 × 17] and (PDB ID:1hd2) [6 × 44 × 33], [15 × 18 × 17] [22]. Meanwhile, possible interactions and ligand orientations were investigated. The energy was reduced for the tested compounds within the specified binding pocket.

2.2.5. Statistical Data Analysis. All experiments were performed independently three times ($n = 3$). The in vitro antibacterial and antioxidant activities of synthetic compounds were expressed as 50% inhibitory concentration (IC_{50}) values. All data were presented as the mean ± standard error of the mean (95% confidence intervals) of three independent experiments. Microsoft Excel 2007 (Roselle, IL, USA) was used for the statistical and graphical analysis. Statistical significance was assessed using a one-way analysis of variance (ANOVA) followed by a *t*-test to determine the degree of significance with the single normal and experimental control group. When the P value < 0.05, differences between data sets were judged statistically significant.

3. Results and Discussion

Considering the pace at which drug resistance is emerging among the pathogens of public health significance, drug design, discovery, and development are the current pressing needs. Researchers around the world are searching for new alternative therapeutic strategies and drug repurposes [23]. This study was done in the search for new small molecules with significant antioxidant and antibacterial activities with a huge potential for new medicine development. Thus, as shown in Scheme 2, a mild and highly efficient process for the synthesis of fused rings of Thiazolo[3,2-α] pyrimidine analogs (**12**–**20**) derived from chalcone via ZnO nanoparticles as a Lewis acid catalyst to activate the carbonyl groups to afford the target products in good to excellent yields (87.9–96.9%). When compared to typical glacial acetic acid-catalyzed reactions under reflux conditions, this approach is experimentally simple, clean, higher yielding, and greener, with improved reaction times. Thus, the green synthesis approach using ZnO nanoparticles as catalysts was found to be an efficient method to synthesize such biologically active compounds compared to the conventional method.

3.1. Recyclability Study of Catalyst. An important investigation into heterogeneous catalysis is the recyclability study. Therefore, good catalysts should be stable and have high activity for scale-up applications. As a result, we looked at the synthesized compound of Thiazolo[3,2-α] pyrimidine analogs' recyclability under ideal reaction conditions. The catalyst was recovered by filtration after the reaction was completed, washed with dichloromethane and methanol, and dried at 100°C for 5 hours before being utilized in the next cycle [24]. The catalyst ZnO-NPs were observed to have good catalytic activity for six consecutive runs with no significant catalytic activity loss and provided the product with a small decrease in reaction yield, as shown in Figure 2 and S3 (Table 3). As presented in S3 (Table 3), ZnO nanoparticles were successfully recovered and reused after the reaction was completed, with no apparent loss of activity, making this process cost-effective and environmentally friendly [23]. When compared to traditional acid catalysts, the efficient utilization of ZnO nanoparticles allows for a faster overall process time and higher product yield by reducing undesirable by-product generation during the reaction [25].

The plausible reaction mechanism for the synthesis of the title compounds, a new synthetic approach utilizing zinc oxide nanoparticles could act as a Lewis acid to activate the carbonyl groups as shown in Scheme 3, resulting in the synthesis of Thiazolo[3,2-α] pyrimidine analogs. It seems like an alkene of α, β-unsaturated ketones (chalcone). After that, the 2-amino thiazole undergoes nucleophilic addition, forming a pyrimidine ring as the amino group of the thiazole, as a Michael donor, attacks the alkene of the, α, β-unsaturated intermediate, making a nucleophilic attack on the β-carbon of the activated chalcone, which is electron deficient due to the electron-withdrawing influence of the carbonyl group, leading to the formation of a Michael type addition product, which is not isolated. The thiazole amino group also attacks the carbonyl group, yielding a cyclocondensation product, which undergoes dehydration to give the target compounds. Finally, ZnO nanoparticles were effectively recovered and reused for numerous runs without apparent loss of activity, making this approach cost-effective and hence environmentally benign.

3.2. General Synthesis. Initially, the synthesis of chalcone derivatives was done at room temperature by combining substituted acetophenone with various substituted aryl aldehydes using a basic catalyzed Claisen–Schmidt condensation reaction, Scheme 4. The substitution pattern at the aryl rings was carefully selected to confer versatile electronic environments, which would certainly affect the antibacterial and antioxidant activity patterns of the target molecules. In the ^{1}H–NMR spectra of compounds, **5**–**7** the H-β and H-α protons appeared each as a doublet at δ 7.7-7.7 and δ 7.3-7.4 respectively, with a coupling constant between them of $^3J = 15.6$ Hz, which agrees with a trans configuration. The

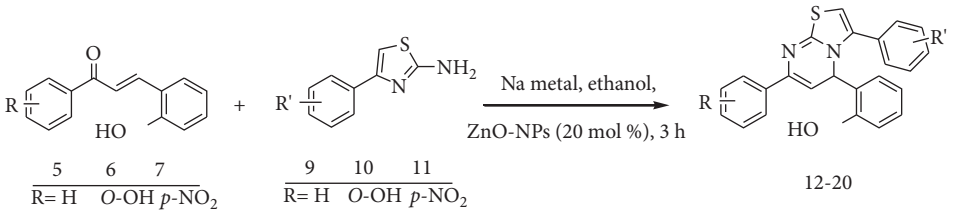

12. R_1= H R_2= H
13. R_1= H R_2= 2-OH
14. R_1= H R_2= 4-NO_2
15. R_1= 4-Br R_2= -H
16. R_1= 4-Br R_2= 2-OH
17. R_1= 4-Br R_2= 4-NO_2
18. R_1= 4-OH R_2= -H
19. R_1= 4-OH R_2= 2-OH
20. R_1= 4-OH R_2= 4-NO_2

Scheme 2: Synthesis of Thiazolo[3,2-α] pyrimidine analogs (**12**–**20**).

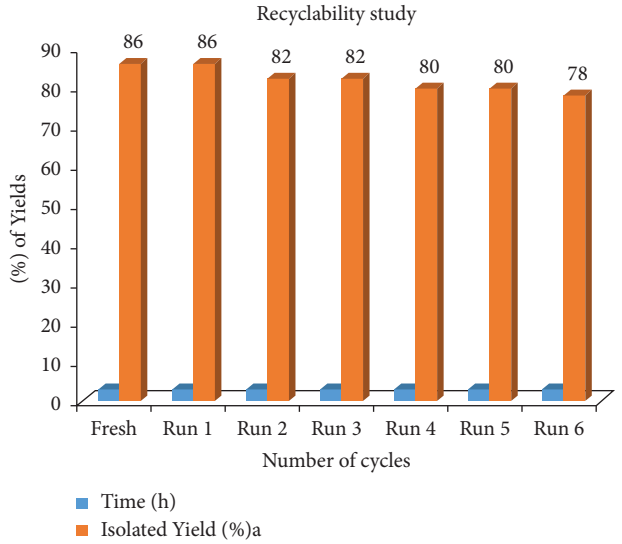

Figure 2: Recyclability investigation for the synthesis of Thiazolo [3,2-α] pyrimidine analogs derived from chalcone catalyzed by ZnO-NPs.

^{1}H–NMR spectrum of synthesized compounds displayed multiplets at δ 7.9–8.5, indicating the aromatic C-H linkage. In the ^{13}C–NMR spectrum for the compounds the C-β and C-α signals appeared at δ 138.4–148.2 and δ 120.1–123.6 ranges respectively, while the C=O appeared at δ 188.9–190.7. All the aromatic carbon peaks appeared in the expected regions (S2 Figure 5 (Appendixes 1–6)).

Thiazole derivatives 9–11 were synthesized as described in Scheme 1. The 4-(4 phenyl substituted) thiazol-2-amine intermediate is obtained by first reacting acetophenone and thiourea in the presence of an iodine catalyst. The 2-amino thiazole derivatives **9**–**11** were synthesized in a single step with good to excellent yields (48.2–96.6%). The singlet in the ^{1}H-NMR spectrum of **9**–**11** was around δ 2.9, confirming the existence of the NH_2 group. As a result of the presence of C-H in the thiazole ring, all compounds displayed singlets at δ 6.9–7.8. The aromatic C-H linkage was revealed by the multiplet at δ 6.9–7.5 in the ^{1}H-NMR spectra of synthesized derivatives. The ^{13}C-NMR spectrum of the thiazole derivatives showed a good agreement with their proposed molecular structure, i.e., the phenyl ring carbons appear around δ 119.2, 127.6, 128.4, 131.2, and 143.3, and signals around δ 107.4, 148.2, and 165.1 are shown for the thiazole ring (S2 (Figure 5) (Appendixes 7–12)).

The synthetic strategy for the preparation of Thiazolo [3,2-α] pyrimidine analogs is illustrated in Scheme 2. Substituted acetophenones were combined with different 2-hydroxy benzaldehyde derivatives in an ethanolic solution of sodium hydroxide to produce the reported chalcone derivatives (**5**–**7**). The target compounds were obtained by reacting either 2-amino-4-substituted phenylthiazole or its substituted derivatives with chalcone derivatives in sodium ethoxide. In this case, acetophenone was used as the ketone of choice and the reaction was also carried out with sodium ethoxide as the solvent. This procedure is efficient for most of the substances used and furnishes the desired product in very good to excellent yields. A 1,4-nucleophilic addition of 2-aminothiazole on, *a* β-unsaturated intermediate resulting from the reaction between the aromatic aldehyde and the molecule bearing the activated methylene group is one proposed reaction mechanism. The respective Thiazolo[3,2-α] pyrimidine analogs were obtained in a synthetically useful manner, then all the obtained products were purified and characterized by UV-Visible, ^{1}H-NMR, and ^{13}C-NMR spectroscopy techniques as depicted in (S2 (Figure 5) (Appendixes 13–30)).

3.3. In Vitro Antibacterial Activities (Agar Disk Diffusion Assay). The antibacterial activity of the nine series of target compounds (**12**–**20**) was evaluated by measuring the size of the zone of inhibition against the test organisms, as depicted in Table 1 and Figure 3. Preliminary evaluation results showed that all synthetic compounds had better antibacterial activity in vitro with mean inhibition zones displayed in the range between 6.33 and 22.33 mm for tested bacterial strains. Results show that among the synthesized analogs, the in vitro antibacterial activity displayed by compound **16** showed higher activity

Table 1: Antibacterial activity of Thiazolo[3,2-α] pyrimidine analogs, **12–20** against selected bacterial strains.

Synthesized compounds		Mean Diameter of inhibition zones (DIZ) in mm			
		Gram-positive bacteria		Gram-negative bacteria	
		Staphylococcus aureus (ATCC 29213)	*Streptococcus pyogenes* (ATCC 27853)	*Escherichia coli* (ATCC 25922)	*Pseudomonas aeruginosa* (ATCC 27853)
12	500 μg/mL	6.67 ± 0.58	9.00 ± 1.00	6.67 ± 0.58	6.33 ± 0.58
	250 μg/mL	8.67 ± 0.58	6.33 ± 0.58	7.33 ± 1.15	9.00 ± 1.00
13	500 μg/mL	8.33 ± 0.58	7.00 ± 0.00	7.33 ± 0.58	11.00 ± 1.00
	250 μg/mL	9.33 ± 1.53	9.33 ± 0.58	6.00 ± 0.00	6.33 ± 0.58
14	500 μg/mL	9.33 ± 0.58	9.00 ± 1.00	12.33 ± 1.15	12.00 ± 1.00
	250 μg/mL	7.33 ± 0.58	6.00 ± 0.00	9.00 ± 0.00	6.33 ± 0.58
15	500 μg/mL	7.33 ± 0.58	8.67 ± 0.58	7.33 ± 0.58	8.00 ± 0.00
	250 μg/mL	8.67 ± 0.58	6.00 ± 0.00	6.00 ± 0.00	6.67 ± 0.58
16	500 μg/mL	10.00 ± 1.00	14.33 ± 1.15	12.67 ± 0.58	14.67 ± 0.58
	250 μg/mL	8.00 ± 0.00	14.33 ± 0.58	8.67 ± 0.58	6.67 ± 0.58
17	500 μg/mL	7.67 ± 0.58	6.67 ± 0.58	7.33 ± 0.58	8.33 ± 0.58
	250 μg/mL	8.33 ± 1.53	7.33 ± 0.58	6.00 ± 0.00	7.67 ± 1.53
18	500 μg/mL	9.33 ± 0.58	8.33 ± 0.58	6.67 ± 0.58	7.33 ± 1.53
	250 μg/mL	6.33 ± 0.58	6.00 ± 0.00	12.33 ± 0.58	12.33 ± 0.58
19	500 μg/mL	12.00 ± 1.73	10.33 ± 0.58	7.67 ± 0.58	8.33 ± 0.58
	250 μg/mL	11.00 ± 1.00	8.67 ± 0.58	6.00 ± 0.00	9.00 ± 1.00
20	500 μg/mL	8.67 ± 0.58	6.33 ± 0.58	12.00 ± 1.00	10.67 ± 1.15
	250 μg/mL	6.00 ± 0.00	6.00 ± 0.00	7.33 ± 0.58	6.33 ± 0.58
Amoxicillin	500 μg/mL	16.33 ± 0.58	27.00 ± 2.00	13.33 ± 1.15	12.33 ± 0.58
	250 μg/mL	14.67 ± 0.58	23.67 ± 2.21	9.33 ± 0.58	9.67 ± 0.58
DMSO		6 ± 0.00	6 ± 0.00	6 ± 0.00	6 ± 0.00

[a]The experiment was carried out in triplicate and the average zone of inhibition was expressed in mean ± standard deviation (mm). [b]N.A. (no activity). [c]ATCC: American tissue culture collection. [d] DIZ: diameter of inhibition zone.

(14.67 ± 0.58 mm at 500 μg/mL) against *P. aeruginosa* compared to amoxicillin (12.33 ± 0.58 mm at 500 μg/mL), whereas compounds **14** and **18** showed comparable activity (12.00 ± 0.00 mm and 12.33 ± 0.58 mm at 500 μg/mL and 250 μg/mL, respectively) against the same strain. Therefore, due to the presence of the electron-donating nature of the *p*-OH substituent on the aromatic ring of the thiazole moiety in compound **16**, it leads to increased anti-bacterial activity against *S. aureus*, *S. pyogenes*, *E. coli,* and *P. aeruginosa* at 500 μg/mL. Compounds **14**, **16**, **18**, and **20** displayed comparable activity (12.33 ± 1.15 mm, 12.65 ± 0.58 mm, 12.33 ± 0.58 mm, 12.00 ± 1.00 mm, respectively, at 500 μg/mL) against *E. coli* compared to amoxicillin (13.33 ± 1.15 mm at the same concentration). Compound **19** showed good activity (12.00 ± 1.72 mm at 500 μg/mL) against *S. aureus* compared to amoxicillin (16.33 ± 0.58 mm at the same concentration). However, the rest of the compounds show low to moderate antibacterial activity against all tested microorganisms at the respective doses, as shown in S3 {Figure 6}.

In terms of structure-activity relationships, the results suggest that the antibacterial activity of the investigated compounds was influenced by the physicochemical properties of the type and position of substituent on the aromatic rings of thiazole and chalcone moieties. The results demonstrate that compound **14**, with a *p*-NO_2 substituent on the aromatic ring of the thiazole moiety, resulted in an increase in antibacterial activity towards *S. aureus, E. coli,* and *P. aeruginosa* at 500 μg/mL compared to compound **12**, which has hydrogen at the para position of the aromatic ring of the thiazole moiety. On the other hand, compound **16**, with a *p*-OH substituent on the aromatic ring of the thiazole moiety, resulted in an increase in antibacterial activity towards *S. aureus, S. pyogenes, E. coli,* and *P. aeruginosa* at 500 μg/mL compared to compound **15**, which has hydrogen at the para position of the aromatic ring of the thiazole moiety. Compound **19**, with a *p*-OH substituent on the aromatic ring of the thiazole moiety, resulted in an increase in antibacterial activity towards *S. aureus* and *S. pyogenes* at 500 μg/mL compared to compound **18,** which has hydrogen at the para position of the aromatic ring of the thiazole moiety, whereas compound **20**, with a *p*-NO_2 substituent on the aromatic ring of the thiazole moiety, resulted in an increasing antibacterial activity trend towards *E. coli* and *P. aeruginosa* at 500 μg/mL compared to compound **18**. The presence of both electron-withdrawing and donating groups in the most active compounds of the thiazole moiety has broad-spectrum activity against the tested Gram-positive and Gram-negative bacterial strains. Thus, the in silico computational studies to predict ADMET and molecular docking analysis of the most active compounds exhibited noncytotoxic and putative binding affinity; these results are in good agreement with their in vitro activities against bacterial species and natural antioxidant agents. The results of the antibacterial activity of all the synthesized compounds are further presented in Figure 3.

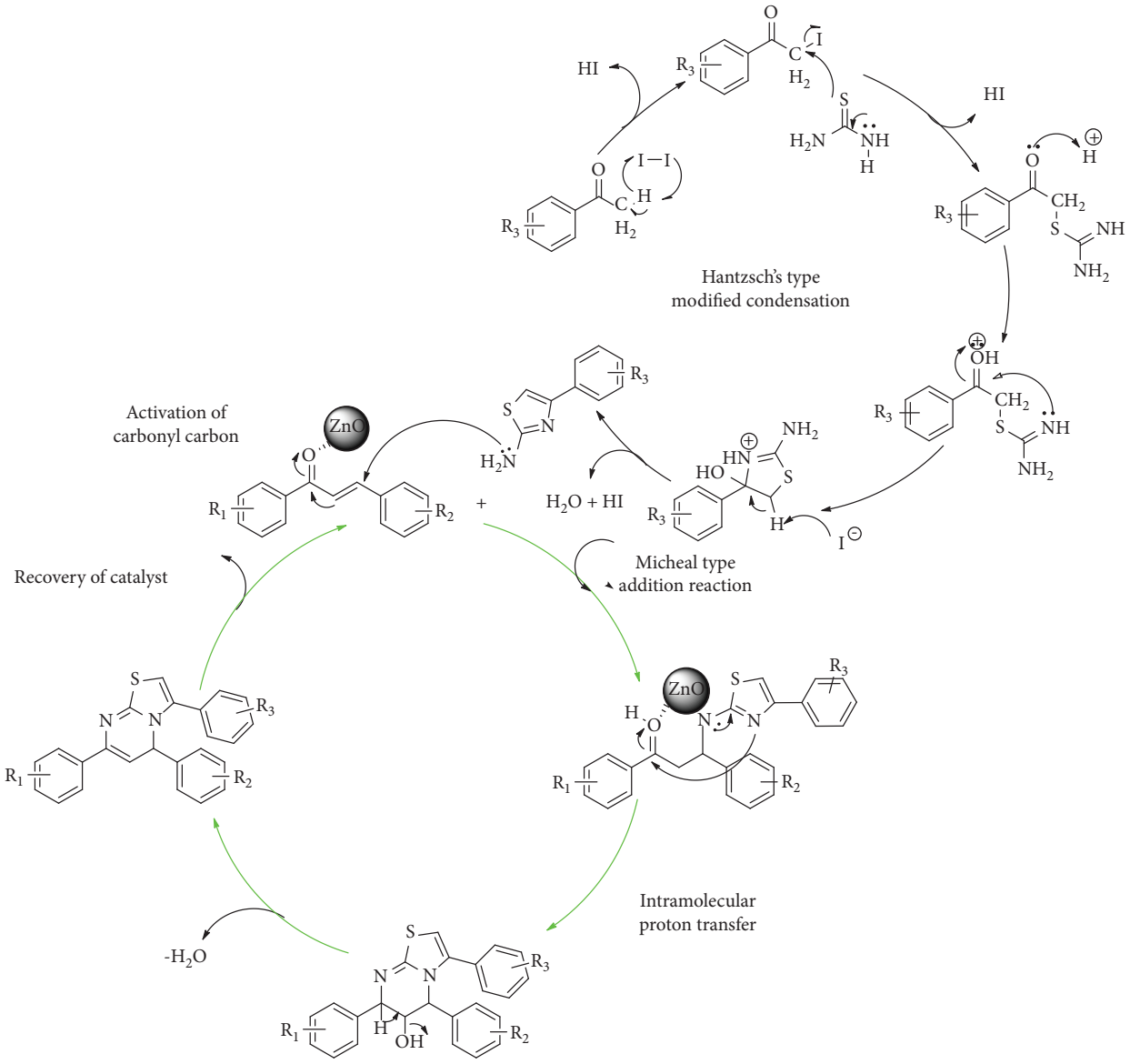

Scheme 3: Plausible reaction mechanism for the synthesis of Thiazolo[3,2-α] pyrimidine analogs via ZnO-nanoparticles as a catalyst.

3.4. In Vitro Antioxidant (DPPH Free Radical Scavenging) Activity. The DPPH free radical scavenging activity is a rapid technique for assessing the ability of synthetic compounds or extracts to scavenge free radicals [26]. Synthesized compounds (**12**–**20**) were assessed for their antioxidant activities as presented in Table 2. The compounds were first screened at five different concentration ranges, namely 12.5, 25.0, 50.0, 100.0, and 200.0 μg/mL (S2 Figure 4). The antioxidant activities were expressed as % DPPH inhibition. IC_{50} was defined as the concentration of sample necessary to inhibit DPPH by 50%. As a result, a lower IC_{50} value suggests that the compound has a stronger ability to operate as a DPPH scavenger and vice versa. As shown in Figure 4, among the tested compounds, compound **19** showed the highest percentage of DPPH inhibition with an IC_{50} value of 9.48 μg/mL compared with the standard drug ascorbic acid (IC_{50} = 3.21 μg/mL). This might be due to the presence of hydroxyl groups at the *ortho*-positions of phenyl rings of thiazole and chalcone moieties that stabilize the radicals for their strong electron-donating nature. The % radical scavenging activity, as well as the IC_{50} values of the synthesized compounds, are shown in Figure 5.

3.5. In Vitro Antilipid Peroxidation Activities. The increased concentration of lipid peroxidation end products increased free radicals, which enhanced the oxidative stress level in living organisms and resulted in cell death. The synthesized compounds (**12**–**20**) were also assessed for their lipid peroxidation potential. As seen in Table 2 and S2 Figure 5, compounds **16** and **19** inhibit peroxide formation by 70.11 ± 0.04 and 76.28 ± 0.12%, demonstrating their potential in preventing the formation of lipid peroxides. However, the synthesized compounds exhibited only a moderate ability to inhibit peroxide formation compared with the natural antioxidant, ascorbic acid. The obtained results

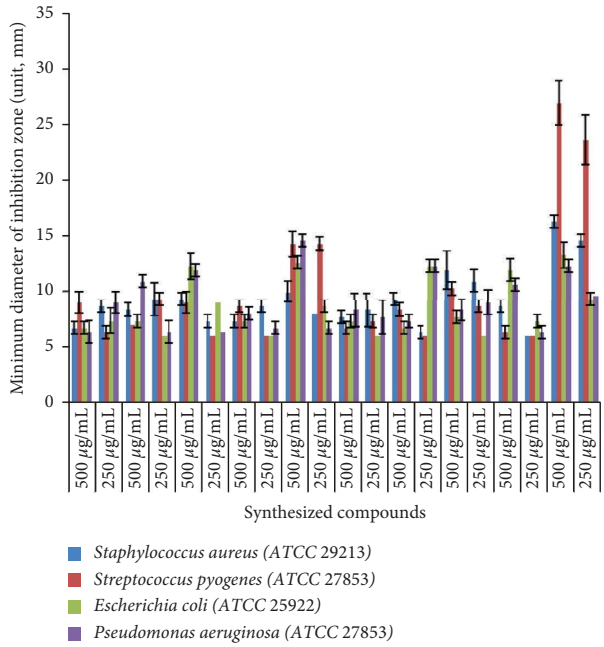

FIGURE 3: Minimum diameter of inhibition zone of the compounds, **12**–**20** in mm (mean ± SD) at 250 and 500 μg/mL concentrations.

showed that the studied Thiazolo[3,2-α] pyrimidine analogs remote the free radicals, especially the lipid peroxide radicals, by giving their hydrogen atom and thus inhibiting the lipid peroxidation reaction. The presence of electron-donating hydroxyl functionality at *ortho*- and *para*-positions of aryl Thiazolo[3,2-α] pyrimidine groups, could be the most possible reason which might stabilize the radicals for their strong electron-donating nature [27].

3.6. In Silico Prediction of Drug-Likeness, and Pharmacokinetic Prediction Study. The therapeutic activity of small molecules depends on their ability to reach the target of interest at sufficient concentrations as defined by the properties of ADMET. As a result, undesired properties of the compound are a primary reason for drug candidate screw-ups in drug discovery at early and late pipeline stages. If these problems could be solved at an early stage, it would be surprisingly useful for the discovery of new drugs [28]. In this study, drug-likeness, pharmacokinetic, and toxicity parameters were estimated for the title synthesized compounds (**12**–**20**) using ADMET descriptors of SwissADME [19], Molinspiration [29], and PreADMET [30] online servers.

The percent absorption of the target compounds was evaluated using the formula %Abs = 109-0.345TPSA [46]. In the filter that combines the drug-likeness criteria of Lipinski's "rule of five" (MW ≤ 500, ilog $P \leq 5$, H-bond donors ≤5, and H-bond acceptors ≤10) [31] and Veber's parameters (TPSA ≤140 Å^2 and rotatable bonds ≤10) [18]. Organ toxicity profiles and ligand toxicological endpoints (AMES (mutagenicity), hERG inhibitors, hepatotoxicity, and skin sensitization) and their LD_{50} were predicted using the Pro Tox II Web Server explorer [32]. The results demonstrated that all compounds, 12–20 showed no violation of Lipinski's rule of five, these zero violations are indicative of their good drug-likeliness as illustrated in Table 3. Furthermore, all synthesized compounds exhibited better bioavailability scores of 0.55, suggesting that they have drug-like properties [33]. Their HBD values (n_{OHNH}) are ˂3, especially in compounds **12**, **14**, **15,** and **17** giving their higher solubility in cellular membranes with also HBA values (n_{ON}) in the range of 2-6, basically for compound **12**. The ilog P values for all compounds below are ˂5, especially for compounds **16** and **18** highlighting their good lipophilic properties. The higher lipophilic nature of these compounds may protect against the harmful effects of ROS and is partly due to their smaller TPSA [34]. TPSA values ranged from 37.53 to 129.17 Å^2, while the consensus log Po/w was observed to range from 2.37 to 3.25. TPSA is a parameter used to predict the transport properties of drugs in passive molecular transport [35]. The tested compounds exhibited better oral absorption than amoxicillin. The compounds have molar refractive index values in the range of 117.77–135.41, suggesting their need in preclinical development and are likely to be drugs.

In addition, the results of the in silico ADME properties compounds (**12**–**20**) show the best results as shown in Table 4. All compounds showed a better intestinal absorption range of 94.625–99.028 showed good intestinal absorption with HIA values close to 100% absorption, especially (**12**, **15,** and **20**). The median permeability of Caco-2 cells in vitro ranged from 12.19 to 55.91, and the permeability of MDCK cells in vitro was low to moderate, with **14**, **15**, **16**, **18,** and **20** being better than amoxicillin (0.39). This indicates that the compound exhibits good absorption properties for passing through the intestinal wall and reaching the target by a passive diffusion mechanism. Skin permeability was found to be slightly below the acceptable range of −4.99 to −5.78 cm/s this corresponds to higher absorption into human skin [36]. Predicted in vivo BBB indicated lower CNS uptake for all compounds, suggesting a lower ability for these compounds to cross the CNS and this indicates these compounds have less capability to cross the CNS with a total clearance value of basically, **16**, **18**, and **20** more than amoxicillin (0.06).

All compounds have strong PPB%, a value greater than 90% indicates strong binding, of which compound **13** (99, 07) in particular showed strong PPB values indicative of prolonged half-lives, more than amoxicillin (23, 35) [37]. In this study, compounds **12**–**20** exhibited no inhibitory behavior against CYP2C19 and CYP3A6 except for **12**, but they did against CYP2C9 and CYP2D4, except for **12**, **14,** and **15**. In addition, glycoprotein inhibition measurements were used to predict the excretion properties of target compounds. P-gp and cytochrome P450 are known to help protect biofilms (gastrointestinal tract or brain) from the efflux (biotransformation) of exogenous substances to protect tissues [38]. In this study, the compounds (**12**–**20**) exhibited non-P-gp substrate inhibition, except **18** and **19**, thus, their liver dysfunction effects are not expected upon administration. Based on toxicity profiles assessed using the PreADMET software, active compounds were screened for carcinogenicity (rat and mouse), mutagenicity, and hERG

Table 2: In vitro antioxidant and antilipid peroxidation inhibition properties of compounds (**12**–**20**).

Conc.(μg/mL)	% of inhibition of the synthesized compounds*									
	12	13	14	15	16	17	18	19	20	Ascorbic acid[a]
12.5	9.85 ± 0.06	26.19 ± 0.99	13.82 ± 0.33	15.12 ± 0.27	30.35 ± 0.30	8.52 ± 0.12	29.23 ± 0.47	32.09 ± 0.03	22.89 ± 0.05	**38.94 ± 0.04**
25.0	21.81 ± 0.32	40.93 ± 0.37	23.83 ± 0.10	31.60 ± 0.05	47.58 ± 0.52	18.70 ± 0.04	41.58 ± 0.14	48.01 ± 0.03	40.21 ± 0.09	**57.16 ± 0.13**
50.0	36.8 ± 0.10	58.9 ± 0.03	37.9 ± 0.24	55.0 ± 0.04	60.4 ± 0.06	29.6 ± 0.05	63.6 ± 0.21	65.6 ± 0.20	59.7 ± 0.15	**77.6 ± 0.18**
100.0	55.64 ± 0.03	70.42 ± 0.12	57.91 ± 0.21	67.89 ± 0.08	72.31 ± 0.03	39.66 ± 0.01	71.74 ± 0.27	78.61 ± 0.06	64.78 ± 0.06	**83.73 ± 0.06**
200.0	60.69 ± 0.23	82.01 ± 0.01	71.54 ± 0.24	79.56 ± 0.51	81.54 ± 0.28	46.27 ± 0.05	80.19 ± 0.06	83.92 ± 0.13	79.70 ± 0.08	**95.71 ± 0.13**
IC_{50} (μg/mL)	128.98	56.02	107.93	78.04	41.72	195.94	46.77	9.48	64.06	**3.21**
% antilipid peroxidation inhibition	56.91 ± 0.37	61.33 ± 0.06	43.65 ± 0.05	67.12 ± 0.04	70.11 ± 0.04	55.43 ± 0.21	49.29 ± 0.52	76.28 ± 0.12	57.19 ± 0.07	**80.34 ± 0.12**

*IC_{50} is the 50% inhibitory concentration of the samples, and the results were represented as mean ± SD. [a]Ascorbic acid was used as a positive control.

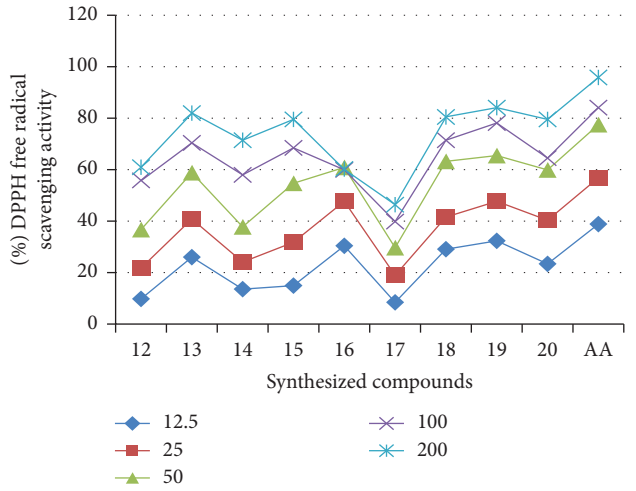

Figure 4: The percent inhibition of the synthesized compounds (**12**–**20**) and the standard drug at the different concentration ranges.

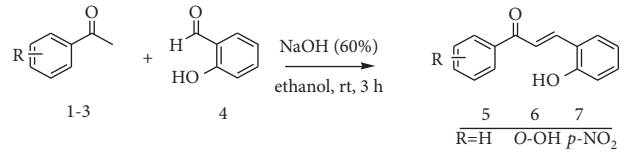

Scheme 4: Synthesis of chalcone derivatives (**5**–**7**).

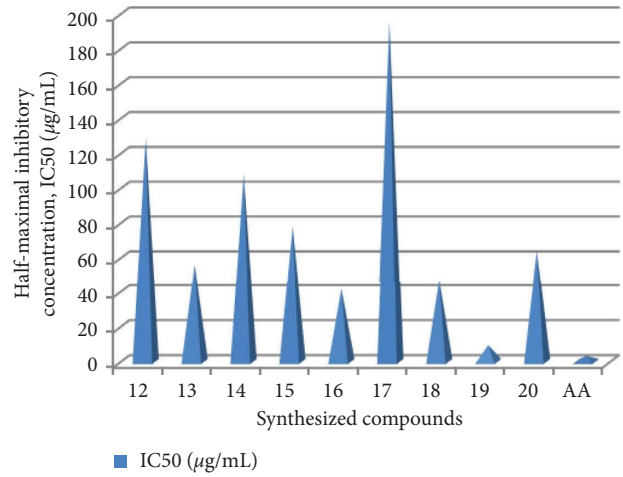

Figure 5: Half-maximal inhibitory concentration (IC50) in μg/mL of synthesized compounds (**12**–**20**) and the standard drug (ascorbic acid).

inhibition in vitro (cardiotoxicity) as shown in Table 5 All compounds showed a positive carcinogenic effect in mice and a negative carcinogenic effect in rats. All compounds were found to be noncardiogenic, noncytotoxic, or safer than amoxicillin, giving it an acceptable profile as a lead for the development of safe and effective drugs in the future. The predicted LD_{50} (mg/kg) for all tested synthetic compounds is 540; therefore, they have been classified by Pro Tox-II as grade 4 toxicity, indicating that the compounds can be harmful if ingested ($300 < LD_{50} \leq 2000$) [39].

The bioavailability radar plots for the tested compounds **12**–**20** (S4 (Figure 1)) indicated that all compounds were located within the pink region, confirming their similarity to the drug with a better bioavailability profile [40]. It exhibits ideal physicochemical properties that make the title compounds good candidates for oral drugs. Despite violating the type Fsp3 <0.25 degree of unsaturation score (INSATU), the compound does not violate the criteria of Lipinski's and Veber's rules and is within the ideal spectrum combined with drug-likeness criteria. The Boiled-Egg server uses wLogP and TPSA to predict these pharmacokinetics [41]. Therefore, the pharmacokinetics were assessed by the boiled egg model (S4 Figure 1) with 12–20, it appeared in the white ellipse (HIA) justifying their high probability to be passively absorbed by the gastro-intestinal tract, with red points **12**, **13**, **14**, **15**, **16**, **17**, and **20** (nonsubstrate of P-gp) and blue point for **18** and **19** (substrate of P-gp), respectively. Interestingly, they are predicted not to be P-gp substrates that provide their promising bioabsorption and bioavailability, which are unable to cross the blood-brain barrier permeability, approving their ability cannot cross the blood-brain barrier to the brain when it binds to specific receptors.

3.7. In Silico Molecular Docking Simulation Study. Molecular docking was considered to be a powerful computational technique in structure-based drug development that allowed the prediction of protein-ligand binding interactions of new molecules at the binding sites of suitable targets of *E. coli* DNA gyrase *B. pyruvate* kinase, PqsA, human peroxiredoxin 5 and explain the associated inhibitory effect. The binding affinity, H-bond, hydrophobic, π-cation/π-anion/π-alkyl, and Van der Waals interactions of ligands were summarized in S4 (Tables 7–11). Most of the target products show promising docking scores and interactions with different amino acid residues (2D and 3D), the results are shown in S5–S9 Figure 1–10. Ribbon model showing the structure of the target protein binding pocket with hydrogen bonds between compounds and amino acids indicated by green dotted lines and hydrophobic interactions indicated by pink lines.

*3.7.1. Molecular Docking Studies of Synthesized Compounds (**12**–**20**) against E. coli DNA Gyrase B (PDB ID: 6f86).* Synthesized compounds (**12**–**20**) were evaluated by molecular docking to bacterial DNA gyrase B, and the results were compared with a standard antibacterial drug (amoxicillin), as shown in S5 (Figure 1–10) and S4 (Table 7), respectively [42]. The minimum binding energies of the synthesized compounds, **12**–**20** ranged from -6.9 to -7.6 kcal/mol, suggesting the inhibitory effect of all compounds against *E. coli* DNA gyrase B. Compared to amoxicillin (−7.1 kcal/mol), synthesized compounds (**12**, **15**, **16,** and **18**) showed better results, and (**14**, **17**, **19**, and **20**) showed similar binding affinity and residual interaction profiles with amino acid residues. The higher binding affinity

Table 3: Calculated parameters of in silico bioavailability (drug-likeness) prediction & physicochemical properties of the synthesized compounds (**12–20**) and amoxicillin.

Compound	MW	iLogP	HBD (n_{OHNH})	HBA (n_{ON})	nrotb	MR	TPSA	% ABS	Lipinski #violations	Synthetic accessibility	Bioavailability score
Lipinski*	≤500	≤5	≤5	≤10				100%			
Veber**	—	—	—	—	≤10		≤140 Å^2			—	
12	382.48	3.25	1	2	3	117.77	37.53	96.05	0	4.48	0.55
13	398.48	2.81	2	3	3	119.79	57.75	89.07	0	4.55	0.55
14	427.48	2.58	1	4	4	126.59	83.35	80.24	0	4.51	0.55
15	427.48	2.78	1	4	4	126.59	83.35	80.24	0	4.51	0.55
16	443.47	2.37	2	5	4	128.61	103.58	73.26	0	4.59	0.55
17	472.47	2.54	1	6	5	135.41	129.17	64.43	0	4.58	0.55
18	398.48	3.19	2	3	3	119.79	57.75	89.07	0	4.54	0.55
19	414.48	2.81	3	4	3	121.81	77.98	82.09	0	4.61	0.17
20	443.47	2.62	2	5	4	128.61	103.58	73.26	0	4.58	0.55
Amoxicillin	365.4	1.46	4	6	5	94.59	132.96	63.12	0	4.17	0.55

*Reference values of Lipinski; **Reference values of Veber; MW, molecular weight; iLogP, lipophilicity (O/W, octanol-water partitioning coefficient); HBD, number of hydrogen bond donors (OH and NH groups); HBA, number of hydrogen bond acceptors (O and N atoms); nVs, number of Lipinski rule violations; nrotb, number of rotatable bonds; MR, molar refractivity; TPSA, topological polar surface area; (Å^2); %ABS, percentage of absorption (% Abs = 109 − [0.345 × TPSA]).

Table 4: Pharmacokinetic (ADME) properties prediction of compounds (**12–20**) and amoxicillin using pre-ADMET online server.

Compound	Absorption				Distribution		Metabolism and excretion				
	HIA (%)[a]	Caco2 (nm/sec)[b]	SPLogKp (cm/hour)[c]	MDCK (nm/sec)[d]	PPB %[e]	BBB (c.brain/c.blood)[f]	CYP2C19[g]	CYP2C9[h]	CYP2D6[i]	CYP3A4[j]	Pgp_inhibition[k]
12	97.153	55.911	−4.99	27.995	96.507	1.0887	Non	Non	Non	Non	Non
13	96.158	41.105	−5.34	12.477	99.071	1.9138	Non	Inhibitor	Non	Inhibitor	Non
14	97.136	27.533	−5.39	0.0691	94.092	0.0161	Non	Inhibitor	Non	Non	Non
15	97.136	20.334	−5.39	0.0572	94.100	0.0161	Non	Inhibitor	Non	Non	Non
16	96.028	12.196	−5.73	0.0561	95.193	0.0218	Non	Inhibitor	Non	Inhibitor	Non
17	96.783	16.635	−5.78	0.0436	95.188	0.0290	Non	Inhibitor	Non	Inhibitor	Non
18	96.158	41.105	−5.34	12.477	93.616	1.9138	Non	Inhibitor	Non	Inhibitor	Inhibitor
19	94.625	23.381	−5.69	4.15085	95.564	2.3180	Non	Inhibitor	Non	Inhibitor	Inhibitor
20	96.028	17.575	−5.73	0.0644	94.514	0.0219	Non	Inhibitor	Non	Inhibitor	Non
Amoxicillin	62.936	0.3483	−9.94	0.3985	23.353	0.0606	Non	Non	Inhibitor	Non	Non

[a] HIA: human intestinal absorption; [b] Caco2: Caco2 cell permeability; [c] SP, LogKp: skin permeability; [d] MDCK: Madin-Darby canine kidney; [e] PBB: plasma protein binding; [f] BBB level: blood-brain barrier level; [g-j] CYP2D6: cytochrome P450 inhibition; [k]P-gp: glycoprotein inhibition.

Table 5: In silico pharmacodynamics (toxicity) prediction of compounds (**12–20**) and amoxicillin using pre-ADMET and Pro Tox-II online servers.

Compound	In silico pharmacodynamics (toxicity)						
	AMES (mutagenicity prediction)	Carcino_Mouse (for carcinogenicity prediction of the tested compounds)	Carcino_Rat (for carcinogenicity prediction of the tested compounds)	hERG_inhibition (for checking the cardiac toxicity)	Cytotoxicity	LD_{50} (mg/kg)	Class
12	Mutagen	Positive	Negative	Low_risk	Negative	540	4
13	Mutagen	Positive	Negative	Low_risk	Negative	540	4
14	Mutagen	Positive	Negative	Low_risk	Negative	540	4
15	Mutagen	Positive	Negative	Low_risk	Negative	540	4
16	Mutagen	Positive	Negative	Low_risk	Negative	540	4
17	Mutagen	Positive	Negative	Low_risk	Negative	540	4
18	Mutagen	Positive	Negative	Low_risk	Negative	540	4
19	Mutagen	Positive	Negative	Low_risk	Negative	540	4
20	Mutagen	Positive	Negative	Low_risk	Negative	540	4
Amoxicillin	Mutagen	Positive	Negative	Low_risk	Negative	540	4

[a]LD_{50}: lethal dose parameter.

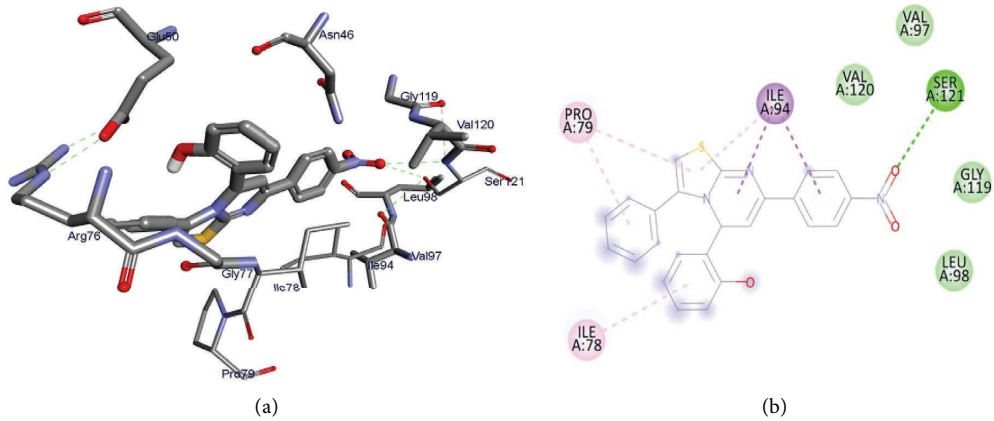

(a) (b)

Figure 6: 3D (b) and 2D (a) representations of the binding interactions of **14** and **16** against E. coli DNA Gyrase B (PDB ID: 6f861).

obtained for compounds **12**, **13**, **15**, and **18** is due to the compounds having a similar hydrogen interaction profile with amino acid residues of Asn-46, Ser-121 and residual interactions Asn-46, Ile-78, and Asp-73, Val-97, Gly-119 (hydrophobic/π-cation/π-anion/π-alkyl or van der Waals interactions) as depicted in Figures 6 and 7. According to the results of molecular docking analysis, all synthesized compounds showed better residual interaction and docking scores than amoxicillin. The docking results (high negative binding affinity) agree well with the in vitro biological activity results of **14** and **16** against *E. coli*.

*3.7.2. Molecular Docking Studies of Synthesized Compounds (**12–20**) against the N-Terminal Domain of PqsA (PDB ID: 5oe3).* The synthesized compounds were subjected to docking analysis to study their binding mode to the *N*-terminal domain of PqsA in a complex with 6-fluoroanthraniloyl-AMP target, and the results were compared with those of standard amoxicillin drugs for comparison, as shown in S6 Figures 1–10 and S4 Table 8 [43]. The synthesized compounds were found to have minimum binding energy between −6.3 to −8.4 kcal/mol in the binding pocket of the *N*-terminal domain of PqsA, with the best result achieved using compounds **15**, **16,** and **18** (−8.4, −8.1 and −8.1 kcal/mol), indicates that the compounds are promising antibacterial agents against *P. aeruginosa*. Compared to amoxicillin (−7.3 kcal/mol), the synthesized compounds (**12**, **13**, **15–17**, **18**, and **19**) have shown better binding affinity and similar amino acid residual interaction profiles. Compounds 15 obtained higher binding affinities due to the interaction of these compounds with amino acid residues Phe-209, Ala-278, Gly-279, Gly-302, Ala-303, His-308, Arg-397, and Asp-382 (hydrophobic/π-cation/π-anion/π-alkane) interactions and van der Waals forces, respectively as presented in Figures 8 and 9. Thus, results of molecular docking are in good correlation with the results of **13**, **16,** and **18** in vitro bioactivity against *P. aeruginosa*.

*3.7.3. Molecular Docking Studies of Synthesized Compounds (**12–20**) against S. aureus Pyruvate Kinase (PDB ID:3t07).* Docking analysis of the synthesized compounds was performed to investigate their binding pattern with Pyruvate Kinase in a complex containing the natural bis-indole alkaloid and the results were compared with standard amoxicillin as shown in S7 Figures 1–10 and S4 Table 9 [44]. The results show that the synthesized compounds have minimum binding energy values in the range from −6.3 to −8.4 kcal/mol in the pyruvate kinase binding pocket, while the best result achieved with compound **15** (−8.4 kcal/mol) indicates that the compounds are promising anti-bacterial agents against *S. aureus* (Figures 10 and 11). Compared to amoxicillin (−4.7 kcal/mol), the synthesized compounds (**12**, **13**, **15–17**, **18**, and **19**) have shown better binding affinities and similar residual interaction profiles with amino acid residues. The higher binding affinity obtained for compounds **13**, **15–17**, **18**, and **19** interact with amino acid residues Ala-358 and residues Phe-209, and Gly-302 via hydrophobic/π-cation/π-anion/π-alkyl, and van der Waals interactions, respectively. The docking results are consistent with the results of **16** and **19** in vitro bioactivity against *S. aureus*.

*3.7.4. Molecular Docking Studies of Synthesized Compounds (**12–20**) against LuxS of S. Pyogenes (PDB ID: P0C0C7).* Docking analysis of the synthesized compounds was performed to examine their binding pattern with LuxS and the results were compared to the amoxicillin drug as shown in S8 Figures 1–10 and S4 Table 10 [45]. The synthesized compounds were found to have minimum binding energies of −4.5 to −6.5 kcal/mol within the binding pocket of LuxS protein. The best results obtained with compound **19** (−6.5 kcal/mol) indicated that these compounds are promising antibacterial agents against *S. pyogenes* (Figures 12 and 13). Compounds, **12–14**, **15**, **17**, and **18-20** have better binding affinity and similar amino acid residual interactions compared to standard amoxicillin drug (−5.7 kcal/mol). The higher binding affinities obtained with compounds **12–14**, **16**, **17**, and **18–20** are amino acid residues Ala-358 and residual interactions Phe-209, and Gly-302. Compounds **16** (Phe-80), **18** (His-61) and **13** (Asn-129) exhibited additional hydrogen and **15** (Pro-79, Arg-83, Cys-127), **16** (His-57, Glu-60, Pro-79, Arg-83), **18** (Leu-56, His-57, Glu-60, Pro-79) remaining interactions,

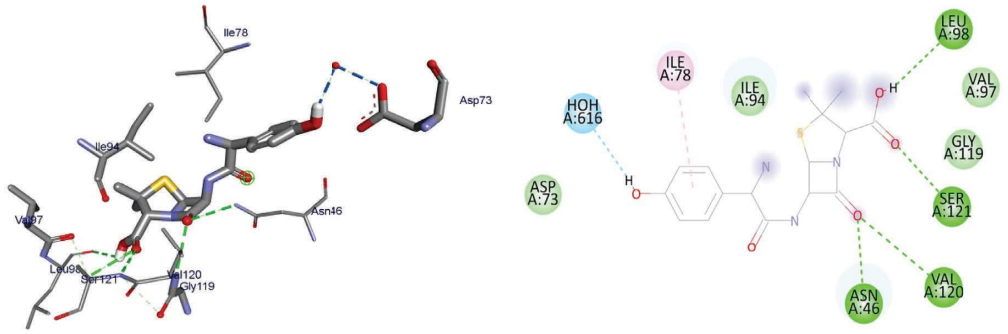

(a) (b)

Figure 7: 3D (b) and 2D (a) representations of the binding interactions of amoxicillin drug against *E. coli* DNA Gyrase B (PDB ID: 6f861).

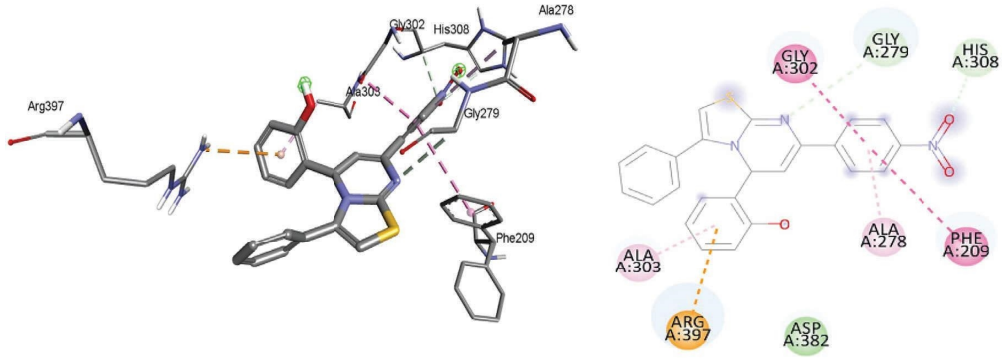

(a) (b)

Figure 8: 3D (b) and 2D (a) representations of the binding interactions of **15** against the *N*-terminal domain of PqsA (PDB ID: 5oe3).

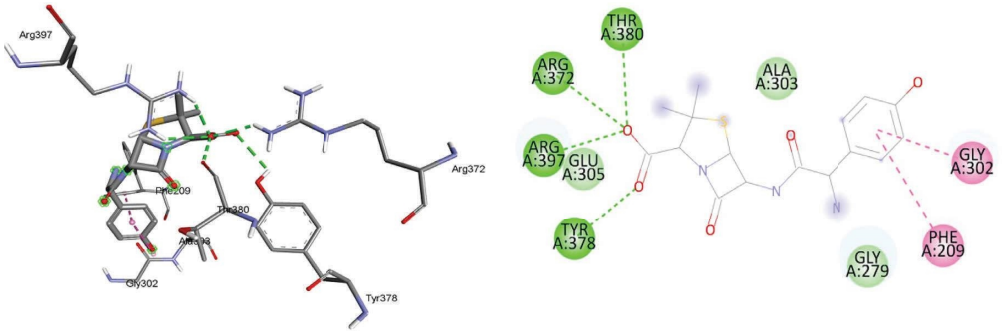

(a) (b)

Figure 9: 3D (b) and 2D (a) representations of the binding interactions of **amoxicillin** against the *N*-terminal domain of PqsA in complex with 6-fluoroanthraniloyl-AMP (crystal form 1) (PDB ID: 5oe3).

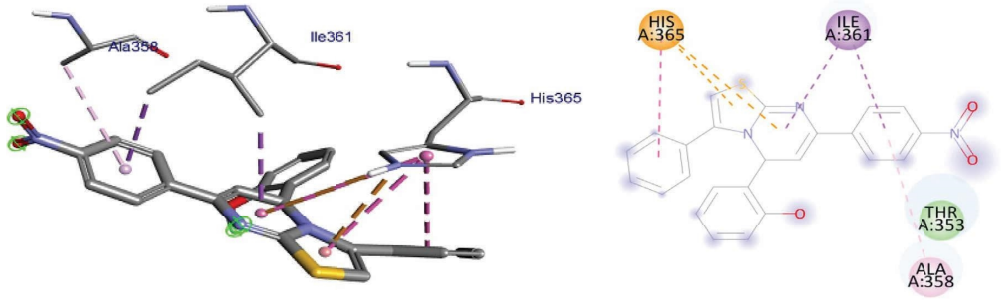

(a) (b)

Figure 10: 3D (b) and 2D (a) representations of the binding interactions of **15** against *S. aureus* pyruvate kinase (PDB ID: 3t07).

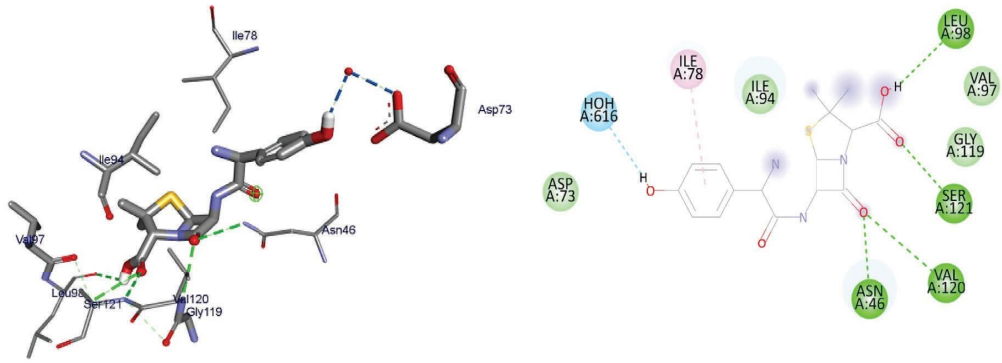

(a) (b)

Figure 11: 3D (b) and 2D (a) representations of the binding interactions of amoxicillin against *S. aureus* pyruvate kinase (PDB ID: 3t07).

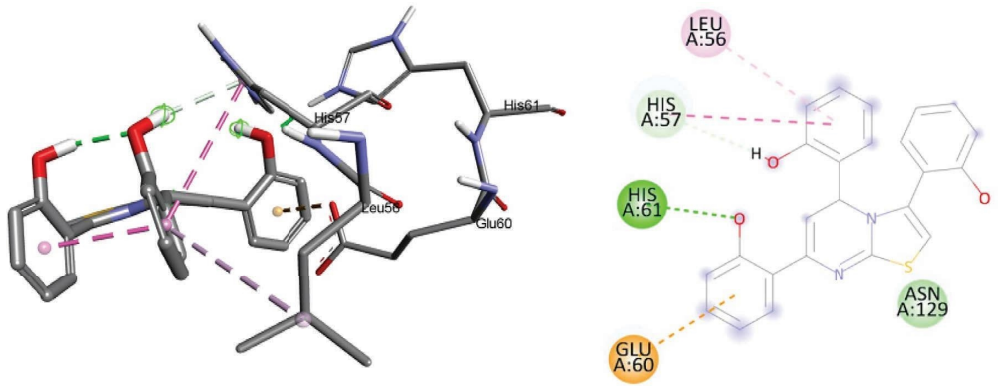

(a) (b)

Figure 12: 3D (b) and 2D (a) representations of the binding interactions of 19 against LuxS of *S. pyogenes* (PDB ID: P0C0C7).

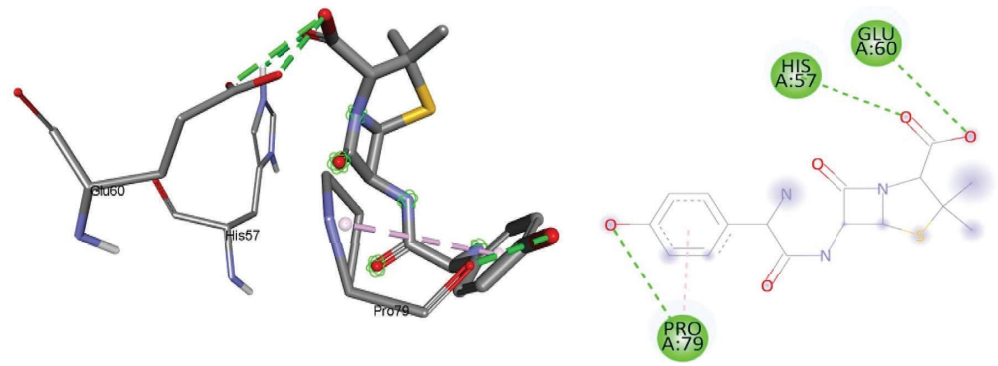

(a) (b)

Figure 13: 3D (b) and 2D (a) representations of the binding interactions of amoxicillin against LuxS of *S. pyogenes* (PDB ID: P0C0C7).

respectively. The results of in silico docking are in good correlation with the results of biological activity against *S. pyogenes*.

*3.7.5. Molecular Docking Studies of Synthesized Compounds (**12**–**20**) against Human Peroxiredoxin 5 (PDB ID: 1hd2).* The molecular docking of target synthetic compounds (**12**–**20**) at the binding site of human peroxidase 5 was also analyzed, and the results were compared with the standard antioxidant ascorbic acid, as shown in S9 (Figures 1–10) and S4 (Table 11). The synthesized compounds were found to have minimum binding energies ranging from −3.0 to −4.8 kcal/mol with a moderate result achieved using compound **12** (−4.8 kcal/mol), which revealed that the compounds are promising antioxidants within the target. Antioxidant analysis of the synthetic compounds showed

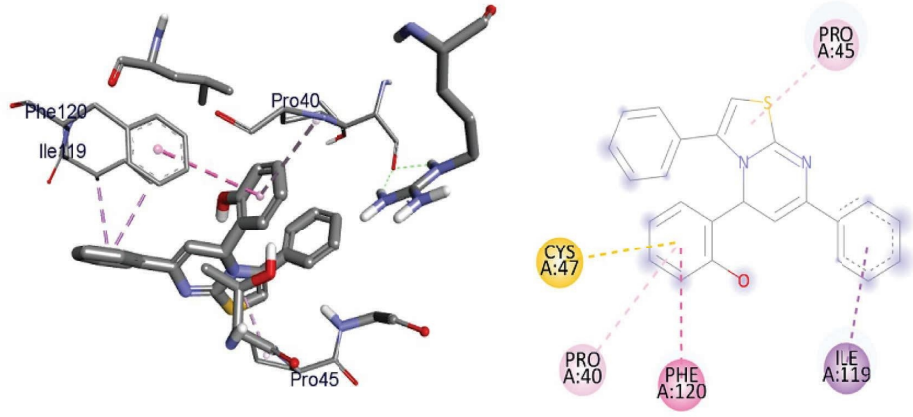

Figure 14: 3D (b) and 2D (a) representations of the binding interactions of **12** against human peroxiredoxin 5 (PDB ID: 1hd2).

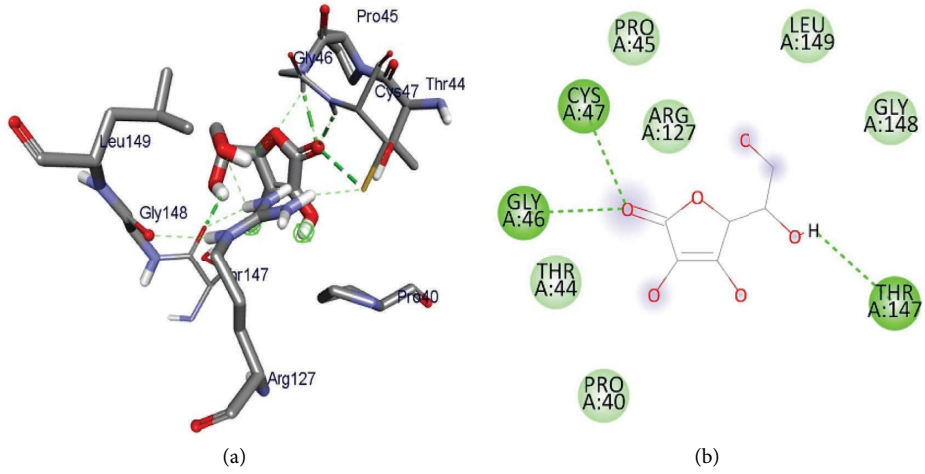

Figure 15: 3D (b) and 2D (a) representations of the binding interactions of ascorbic acid against human peroxiredoxin 5 (PDB ID: 1hd2).

moderate to good activity. In addition, all compounds showed relevant binding affinity and residual interaction for vitamin C, as shown in Figures 14 and 15.

4. Conclusions

In this study, we reported an efficient and greener approach toward the synthesis of nine series of fused rings of Thiazolo [3,2-α] pyrimidine analogs catalyzed by ZnO nanoparticles. Among the synthesized analogs, compound **16** showed higher activity at 500 μg/mL against *P. aeruginosa* compared to amoxicillin at the same dose, whereas compounds **14** and **18** showed comparable activity at 500 μg/mL and 250 μg/mL, respectively, against the same strain. Compounds **14**, **16**, **18,** and **20** displayed comparable activity at 500 μg/mL against *E. coli* compared to amoxicillin at the same concentration. Compound **19** showed good activity at 500 μg/mL against *S. aureus* compared to amoxicillin at the same concentration. Compound **19** displayed the highest percent inhibition of DPPH with an IC_{50} value of 9.48 g/mL compared to ascorbic acid (3.21 g/mL) and showed promising inhibition of peroxide formation by 76.28 ± 0.12%, indicating their potential in preventing the formation of lipid peroxides. Molecular docking analysis of compounds **14**, **16**, **18**, and **20** revealed promising DNA Gyrase B inhibitory effects with the binding affinity of −7.1, −7.3, −7.6, and −6.9 Kcal/mol, respectively, and compounds **16, 18,** and **19** displayed binding affinities of −8.1, −8.1, and −7.2 Kcal/mol, respectively, against PqsA, compared to amoxicillin (−7.1 and −7.3 Kcal/mol, respectively). These results are in correlation with the in vitro antibacterial activities displayed by these compounds against *E. coli* and *P. aeruginosa.* Compound **19** displayed a binding affinity of −3.6 Kcal/mol against human peroxiredoxin 5 compared to ascorbic acid (−5.2 Kcal/mol). In vitro biological activities and in silico computational results revealed that compounds **14**, **16,** and **18** are good antibacterial agents against *P. aeruginosa* and *E. coli*, whereas compound **19** was found to be a promising antibacterial agent against *S. aureus* and antioxidant agents. Consequently, in silico ADMET predictions and molecular docking studies of synthesized compounds showed strong

agreement with the in vitro studies of antibacterial and antioxidant biological results, suggesting the synthesized compounds appear to be lead compounds for rational drug design.

Abbreviations

TLC: Thin layer chromatography
AA: Ascorbic acid
AMR: Antimicrobial resistance
ROS: Reactive oxygen species
ADMET: Absorption, distribution, metabolism, excretion, and toxicity
ANOVA: Analysis of variance
ZnO-NPs: Zinc Oxide nanoparticles
DPPH: 1,1-diphenyl-2-picrylhydrazyl
IC_{50}: Inhibitory concentration inhibiting 50% of growth
NMR: Nuclear magnetic resonance
DIZ: Diameter of inhibition zone
RSA: Radical scavenging activity
UV: Ultraviolet
FT-IR: Fourier transmission infrared spectroscopy
XRD: X-ray diffraction
TEM: Transmission electron microscopy
PL: Photoluminescence
TGA: Thermo gravimetric analysis
TMS: Tetramethylsilane
MeOH: Methanol
PE: Petroleum ether
CLSI: Clinical and Laboratory Standards Institute's standard protocols
SMILEs: Simplified molecular-input line-entry system
PDB ID: Protein data bank identity
SAR: Structure-activity relationships
DMSO: Dimethyl sulfoxide
E. coli: *Escherichia coli*
S. aureus: Staphylococcus aureus
P. aeruginosa: Pseudomonas aeruginosa
S. pyogenes: Streptococcus pyogenes.

Data Availability

The data used to support the findings of this study are included within the manuscript and supplementary information.

Conflicts of Interest

The authors declare that they have no conflicts of interest regarding the publication of this paper.

Authors' Contributions

DZ designed the work, carried out the experimental part, synthesized and analyzed the experimental data, and wrote the original manuscript. ME supervised the study design and experimental work and participated in data analysis, interpretation, and manuscript critical review. YM participated in experimental work, data analysis, and manuscript review. JOO and TBD conducted the NMR analysis and interpretations and manuscript edition. RE assisted in biological and molecular docking calculations and analysis. All the authors read and approved the final manuscript.

Acknowledgments

The authors acknowledged the Department of Applied Chemistry, the School of Applied Natural Science, the Adama Science and Technology University, and the Wachemo University for Ph.D. opportunity study and leave of absence, respectively. The support rendered by the Adama Public Health Research & Referral Laboratory Center, Adama, Ethiopia, during the antibacterial study is gratefully acknowledged.

Supplementary Materials

The UV-Visible, ^{1}H, and ^{13}C-NMR spectra of all the synthesized compounds, molecular docking scores, and 3D and 2D representations of the binding interactions of synthesized compounds, **12**–**20** and amoxicillin/ascorbic acid against target proteins (i.e., DNA gyrase B, PqsA, LuxS, Pyruvate Kinase, and Human peroxiredoxin 5), bioavailability radar, and the Boiled-Egg model of the compounds (**12**–**20**) are all presented in the supplementary information. (*Supplementary Materials*)

References

[1] F. Prestinaci, P. Pezzotti, and A. Pantosti, "Antimicrobial resistance: a global multifaceted phenomenon," *Pathogens and Global Health*, vol. 109, no. 7, pp. 309–318, 2015.

[2] S. Dhingra, N. A. A. Rahman, E. Peile et al., "Microbial resistance movements: an overview of global public health threats posed by antimicrobial resistance, and how best to counter," *Frontiers in Public Health*, vol. 8, Article ID 535668, 2020.

[3] H. Van Acker and T. Coenye, "The role of reactive oxygen species in antibiotic-mediated killing of bacteria," *Trends in Microbiology*, vol. 25, no. 6, pp. 456–466, 2017.

[4] G. Prabakaran, S. Manivarman, and M. Bharanidharan, "Catalytic synthesis, ADMET, QSAR and molecular modeling studies of novel chalcone derivatives as highly potent antioxidant agents," *Materials Today Proceedings*, vol. 48, pp. 400–408, 2022.

[5] A. M. S. Youssef, A. M. Fouda, and R. M. Faty, "Microwave assisted synthesis of some new thiazolopyrimidine and pyrimidothiazolopyrimidopyrimidine derivatives with potential antimicrobial activity," *Chemistry Central Journal*, vol. 12, pp. 50–14, 2018.

[6] U. K. Bhadraiah, V. Basavanna, D. M. Gurudatt, R. P. Shivalingappa, and N. S. Lingegowda, "Bicyclic [1, 3, 4] Thiadiazolo [3, 2-α] pyrimidine analogues: novel one-pot three-component synthesis, antimicrobial, and antioxidant evaluation," 2021.

[7] F. Wu, Y. Luo, and C. Hu, *Recent Progress in the Synthesis of Thiazolo [3, 2-a] Pyrimidine Compounds*, IOP Publishing, Bristol, UK, 2018.

[8] B. Banerjee, "Recent developments on nano-ZnO catalyzed synthesis of bioactive heterocycles," *Journal of Nanostructure in Chemistry*, vol. 7, no. 4, pp. 389–413, 2017.

[9] M. G. Demissie, F. K. Sabir, G. D. Edossa, and B. A. Gonfa, "Synthesis of zinc oxide nanoparticles using leaf extract of lippia adoensis (koseret) and evaluation of its antibacterial activity," *Journal of Chemistry*, vol. 2020, 9 pages, 2020.

[10] P. Yadav, K. Lal, A. Kumar, S. K. Guru, S. Jaglan, and S. Bhushan, "Green synthesis and anticancer potential of chalcone linked-1, 2, 3-triazoles," *European Journal of Medicinal Chemistry*, vol. 126, pp. 944–953, 2017.

[11] J. Zitko, O. Jand'ourek, P. Paterová et al., "Design, synthesis and antimycobacterial activity of hybrid molecules combining pyrazinamide with a 4-phenylthiazol-2-amine scaffold," *Medicinal Chemistry Communications*, vol. 9, no. 4, pp. 685–696, 2018.

[12] F. Lemilemu, M. Bitew, T. B. Demissie, R. Eswaramoorthy, and M. Endale, "Synthesis, antibacterial and antioxidant activities of Thiazole-based Schiff base derivatives: a combined experimental and computational study," *BMC Chemistry*, vol. 15, pp. 67–18, 2021.

[13] J. Hudzicki, "Kirby-Bauer disk diffusion susceptibility test protocol," *American Society for Microbiology*, vol. 15, pp. 55–63, 2009.

[14] D. H. Bergey, *Bergey's Manual of Determinative Bacteriology*, Lippincott Williams & Wilkins, Philadelphia, PA, USA, 1994.

[15] J. N. Eloff, "Avoiding pitfalls in determining antimicrobial activity of plant extracts and publishing the results," *BMC Complementary and Alternative Medicine*, vol. 19, pp. 106–108, 2019.

[16] F. Ullah, N. Iqbal, M. Ayaz et al., "DPPH, ABTS free radical scavenging, antibacterial and phytochemical evaluation of crude methanolic extract and subsequent fractions of *Chenopodium botrys* aerial parts," *Pakistan Journal of Pharmaceutical Sciences*, vol. 30, no. 3, pp. 761–766, 2017.

[17] W. A. Yehye, N. Abdul Rahman, A. A Alhadi, H. Khaledi, S. W. Ng, and A. Ariffin, "Butylated hydroxytoluene analogs: synthesis and evaluation of their multipotent antioxidant activities," *Molecules*, vol. 17, no. 7, pp. 7645–7665, 2012.

[18] D. F. Veber, S. R. Johnson, H.-Y. Cheng, B. R. Smith, K. W. Ward, and K. D. Kopple, "Molecular properties that influence the oral bioavailability of drug candidates," *Journal of Medicinal Chemistry*, vol. 45, no. 12, pp. 2615–2623, 2002.

[19] A. Daina, O. Michielin, and V. Zoete, "SwissADME: a free web tool to evaluate pharmacokinetics, drug-likeness and medicinal chemistry friendliness of small molecules," *Scientific Reports*, vol. 7, pp. 42717–42813, 2017.

[20] A. Ah and A. Yi, "In silico pharmacokinetics and molecular docking studies of lead compounds derived from *Diospyros mespiliformis*," *Pharma*, vol. 7, no. 3, pp. 31–37, 2019.

[21] D. Seeliger and B. L. de Groot, "Ligand docking and binding site analysis with PyMOL and Autodock/Vina," *Journal of Computer-Aided Molecular Design*, vol. 24, no. 5, pp. 417–422, 2010.

[22] O. Trott and A. J. Olson, "AutoDock Vina: improving the speed and accuracy of docking with a new scoring function, efficient optimization, and multithreading," *Journal of Computational Chemistry*, vol. 31, no. 2, pp. 455–461, 2010.

[23] L. M. Streicher, "Exploring the future of infectious disease treatment in a post-antibiotic era: a comparative review of alternative therapeutics," *Journal of Global Antimicrobial Resistance*, vol. 24, pp. 285–295, 2021.

[24] M. J Piltan and J. S Ghomi, "Nano crystalline ZnO catalyzed one pot three-component synthesis of 7-alkyl-6H, 7H-naphtho [1', 2': 5, 6] pyrano [3, 2-c] chromen-6-ones under solvent-free conditions," *Bulletin of the Chemical Society of Ethiopia*, vol. 30, no. 2, pp. 289–296, 2016.

[25] A. Aldalbahi, S. Alterary, R. Ali Abdullrahman Almoghim et al., "Greener synthesis of zinc oxide nanoparticles: characterization and multifaceted applications," *Molecules*, vol. 25, no. 18, p. 4198, 2020.

[26] H. Bouherrou, A. Saidoun, A. Abderrahmani et al., "Synthesis and biological evaluation of new substituted hantzsch thiazole derivatives from environmentally benign one-pot synthesis using silica supported tungstosilisic acid as reusable catalyst," *Molecules*, vol. 22, no. 5, p. 757, 2017.

[27] M. S. Shah, M. M. Rahman, M. D. Islam et al., "Synthesis, antimicrobial and antioxidant evaluation with in silico studies of new thiazole Schiff base derivatives," *Journal of Molecular Structure*, vol. 1248, Article ID 131465, 2022.

[28] P. Abishad, P. Niveditha, V. Unni et al., "In silico molecular docking and in vitro antimicrobial efficacy of phytochemicals against multi-drug-resistant enteroaggregative *Escherichia coli* and non-typhoidal Salmonella spp," *Gut Pathogens*, vol. 13, pp. 46–11, 2021.

[29] T. B. Hadda, V. Rastija, F. AlMalki et al., "Petra/osiris/molinspiration and molecular docking analyses of 3-Hydroxy-Indolin-2-one derivatives as potential antiviral agents," *Current Computer-Aided Drug Design*, vol. 17, no. 1, pp. 123–133, 2021.

[30] S. Lee, I. Lee, H. Kim, G. Chang, and J. Chung, "The Pre-ADME approach: web-based program for rapid prediction of physico-chemical, drug absorption and drug-like properties," in *Proceedings of the EuroQSAR 2002 Designing Drugs and Crop Protectants: Processes, Problems and Solutions*, pp. 418–420, Massachusetts, MA, USA, 2003.

[31] C. A. Lipinski, F. Lombardo, B. W. Dominy, and P. J. Feeney, "Experimental and computational approaches to estimate solubility and permeability in drug discovery and development settings," *Advanced Drug Delivery Reviews*, vol. 23, no. 1–3, pp. 3–25, 1997.

[32] P. Banerjee, A. O. Eckert, A. K. Schrey, and R. Preissner, "ProTox-II: a webserver for the prediction of toxicity of chemicals," *Nucleic Acids Research*, vol. 46, no. W1, pp. W257–W263, 2018.

[33] Y. C. Martin, "A bioavailability score," *Journal of Medicinal Chemistry*, vol. 48, no. 9, pp. 3164–3170, 2005.

[34] A. Daina, O. Michielin, and V. Zoete, "iLOGP: a simple, robust, and efficient description of n-octanol/water partition coefficient for drug design using the GB/SA approach," *Journal of Chemical Information and Modeling*, vol. 54, no. 12, pp. 3284–3301, 2014.

[35] P. Ertl, B. Rohde, and P. Selzer, "Fast calculation of molecular polar surface area as a sum of fragment-based contributions and its application to the prediction of drug transport properties," *Journal of Medicinal Chemistry*, vol. 43, no. 20, pp. 3714–3717, 2000.

[36] F. Zafar, A. Gupta, K. Thangavel et al., "Physicochemical and pharmacokinetic analysis of anacardic acid derivatives," *ACS Omega*, vol. 5, no. 11, pp. 6021–6030, 2020.

[37] C. Alonso, V. Carrer, S. Espinosa et al., "Prediction of the skin permeability of topical drugs using in silico and in vitro models," *European Journal of Pharmaceutical Sciences*, vol. 136, Article ID 104945, 2019.

[38] A. Finch and P. Pillans, "P-glycoprotein and its role in drug-drug interactions," *Australian Prescriber*, vol. 37, no. 4, pp. 137–139, 2014.

[39] M. N. Drwal, P. Banerjee, M. Dunkel, M. R. Wettig, and R. Preissner, "ProTox: a web server for the in silico prediction of rodent oral toxicity," *Nucleic Acids Research*, vol. 42, no. W1, pp. W53–W58, 2014.

[40] M. A. Islam and T. S. Pillay, "Identification of promising anti-DNA gyrase antibacterial compounds using de novo design, molecular docking and molecular dynamics studies," *Journal of Biomolecular Structure & Dynamics*, vol. 38, no. 6, pp. 1798–1809, 2020.

[41] A. Daina and V. Zoete, "A boiled-egg to predict gastrointestinal absorption and brain penetration of small molecules," *ChemMedChem*, vol. 11, pp. 1117–1121, 2016.

[42] N. H. Metwally, S. O. Abdallah, and M. M. A. Mohsen, "Design, green one-pot synthesis and molecular docking study of novel *N*, *N*-bis (cyanoacetyl) hydrazines and bis-coumarins as effective inhibitors of DNA gyrase and topoisomerase IV," *Bioorganic Chemistry*, vol. 97, Article ID 103672, 2020.

[43] F. Witzgall, W. Ewert, and W. Blankenfeldt, "Structures of the *N*-terminal domain of PqsA in complex with anthraniloyl- and 6-fluoroanthraniloyl-AMP: substrate activation in Pseudomonas quinolone signal (PQS) biosynthesis," *ChemBioChem*, vol. 18, no. 20, pp. 2045–2055, 2017.

[44] C. G. L. Veale, R. Zoraghi, R. M. Young et al., "Synthetic analogues of the marine bisindole deoxytopsentin: potent selective inhibitors of MRSA pyruvate kinase," *Journal of Natural Products*, vol. 78, no. 3, pp. 355–362, 2015.

[45] L. Zhou, Y. Zhang, Y. Ge, X. Zhu, and J. Pan, "Regulatory mechanisms and promising applications of quorum sensing-inhibiting agents in control of bacterial biofilm formation," *Frontiers in Microbiology*, vol. 11, Article ID 589640, 2020.